LBL-14275
c.2

Lawrence Berkeley Laboratory

UNIVERSITY OF CALIFORNIA

RECEIVED
LAWRENCE
BERKELEY LABORATORY

JUN 18 1982

LIBRARY AND
DOCUMENTS SECTION

Materials & Molecular Research Division

QUANTUM NOISE IN JOSEPHSON JUNCTIONS AND DC SQUIDS

Roger Hilsen Koch
(Ph.D. thesis)

May 1982

TWO-WEEK LOAN COPY

This is a Library Circulating Copy which may be borrowed for two weeks. For a personal retention copy, call Tech. Info. Division, Ext. 6782.

LBL-14275
c.2

Prepared for the U.S. Department of Energy under Contract DE-AC03-76SF00098

DISCLAIMER

This document was prepared as an account of work sponsored by the United States Government. While this document is believed to contain correct information, neither the United States Government nor any agency thereof, nor the Regents of the University of California, nor any of their employees, makes any warranty, express or implied, or assumes any legal responsibility for the accuracy, completeness, or usefulness of any information, apparatus, product, or process disclosed, or represents that its use would not infringe privately owned rights. Reference herein to any specific commercial product, process, or service by its trade name, trademark, manufacturer, or otherwise, does not necessarily constitute or imply its endorsement, recommendation, or favoring by the United States Government or any agency thereof, or the Regents of the University of California. The views and opinions of authors expressed herein do not necessarily state or reflect those of the United States Government or any agency thereof or the Regents of the University of California.

LBL-14275

QUANTUM NOISE IN JOSEPHSON JUNCTIONS AND DC SQUIDS

Roger Hilsen Koch

Department of Materials and Molecular Research
Lawrence Berkeley Laboratory
University of California
Berkeley, California 94720

May 1982

This work was supported by the Director, Office of Energy Research, Office of Basic Energy Sciences, Materials Sciences Division of the U.S. Department of Energy under Contract No. DE-AC03-76SF00098.

QUANTUM NOISE IN JOSEPHSON JUNCTIONS AND DC SQUIDS

Roger Hilsen Koch

Abstract

The development of a model to predict and understand the effects of quantum noise in the resistively shunted Josephson junction and experimental tests of this model are described. It is shown that the low-frequency spectral density of the voltage noise in a current-biased Josephson junction with critical current I_o, shunt resistance R, and small capacitance is $2eI_o^2R^3/V$ in the limit $eV \gg k_BT(I/I_o)^2$ and $I > I_o$, where V is the voltage and I is the current. The noise arises from zero-point current fluctuations in the shunt resistor that are mixed down from near the Josephson frequency to the much lower measurement frequency. Experimental data are in excellent agreement with these predictions, demonstrating clearly the measurability of zero-point fluctuations and the validity when $I > I_o$ of the Langevin treatment combined with the Callen-Welton expression for the noise from a resistor. The rounding of the current-voltage characteristic when $I \lesssim I_o$ caused by quantum noise and macroscopic quantum effects are briefly discussed.

The noise temperature of a dc superconducting quantum interference device (SQUID) coupled to a tuned input circuit is computed using the complete quantum expression for the equilibrium noise in the shunt resistance of each junction. At T = 0, where the noise reduces to zero-point fluctuations, the noise temperature for an optimized system is $h\nu/k_B\ln 2$, where ν is the signal frequency and the noise energy, ε/1Hz, of the bare SQUID is approximately $\approx \hbar$. The computation is extended to

nonzero temperatures, and it is shown that a SQUID operated at 1K can approach the quantum limit. Tunnel junction dc SQUIDs designed to approach the quantum noise limit in the temperature range 1 to 4K were fabricated with an inductance of about 2 pH and a capacitance per junction of about 0.5 pF. The lowest measured noise energy was $3.2\hbar$ at 1.4K at a frequency of 202 kHz. When the 1/f noise was subtracted, the white noise energy decreased from around $3\hbar$ at 4.2K to below $2\hbar$ at 1.4K.

ACKNOWLEDGMENTS

I wish to thank my research advisor, Professor John Clarke, for his timely advice, his opinions on ideas and many interesting conversations about Physics and other things. The fabrication help of Dr. Dale Van Harlingen was invaluable; I thank him for this and his many other contributions to the quantum noise probject. Finally, I wish to thank all my colleagues in the Clarke group and Greg Swift for their relatively high tolerance to noise.

This work was supported by the Director, Office of Energy Research, Office of Basic Energy Sciences, Materials Sciences Division of the U.S. Department of Energy under Contract No. DE-AC03-76SF00098.

TABLE OF CONTENTS

	Page
INTRODUCTION	1
SINGLE JUNCTION THEORY	6
SINGLE JUNCTION MEASUREMENTS	21
DC SQUID THEORY	56
DC SQUID MEASUREMENTS	67
APPENDIX A: COMPUTER METHODS	76
APPENDIX B: TIGHTLY COUPLED SQUIDS	83
APPENDIX C: MACROSCOPIC QUANTUM EFFECTS	87
REFERENCES	93

I. INTRODUCTION

We wish to analyze the problem of a current-biased Josephson junction (Josephson, 62) shunted with a resistor and the junction's intrinsic self-capacitance. The parameter we can vary after the junction is fabricated is the bias current. We will predict and measure the average voltage across the junction and the low frequency fluctuations around the average. This problem is sufficiently complicated to justify two starting models; (1) the 'simple' Resistively Shunted Junction (RSJ) model (Stewart, 68; McCumber, 68) i.e., the electrical engineering approach, and (2) the transfer Hamiltonian method (Ferrell and Prange, 63; Anderson, 64) which is based in quantum mechanics and is far more complicated but can be shown to reduce exactly to the RSJ model in most circumstances.

The RSJ model is used by most workers in the field because of its simplicity and predictive abilities. All the following chapters of this thesis will unabashedly use the RSJ model for predictions and in all cases the measured data are in good agreement with these predictions.

The RSJ model has been thoroughly tested in the thermal limit when $k_BT > h\nu_J$ where ν_J is the Josephson frequency. The essential idea presented and tested successfully is that these non-linear classical Langevin equations of motion remain valid in most cases when $h\nu_J > k_BT$, the 'quantum' limit provided that the thermal terms in the equations of motion are replaced by their quantum mechanical analogies. This means changing the spectrum of the Langevin driving term representing the resistor noise, from the thermal Johnson noise formula (Johnson,

28; Nyquist, 28) for the voltage noise,

$$S_V(\nu) = 4K_BTR, \tag{1.1}$$

to the complete quantum formulation (Callen and Welton, 51):

$$S_V(\nu) = 2h\nu R \coth(h\nu/2K_BT) \tag{1.2}$$

In Chapter II we will present the quantum noise theory of the single junction, using the RSJ model. Appendix A presents some details of the computer methods. Chapter III will report on the results of the measurements; they are in excellent agreement with the theory and for the first time experimentally verify equation (1.2). These measurements tested the model when $I > I_o$ (the current bias I was greater than I_o, the maximum possible pair current through the junction).

Having tested these ideas in the single junction, we make predictions for the performances of the dc SQUID, which is, roughly speaking, two junctions wired together. We find that at attainable temperatures and present-day technologies the dc SQUID when configured as a narrow-band amplifier can be an ideal phase-preserving linear amplifier, i.e. the best possible allowed by quantum mechanics. This means it would have a total equivalent noise power per unit bandwidth equal to $h\nu_m$ referred to the input (ν_m is the measurement frequency). The frequency range over which we obtain quantum-limited performance is approximately 1 MHz to 1+GHz. This is much lower than any other equivalent amplifier.

The calculational results also predict a minimum noise energy of the dc SQUID of approximately $\hbar$. The race to reach this or any ultimate limit' is depicted in Figure 1.1. The noise energy, or energy resolu-

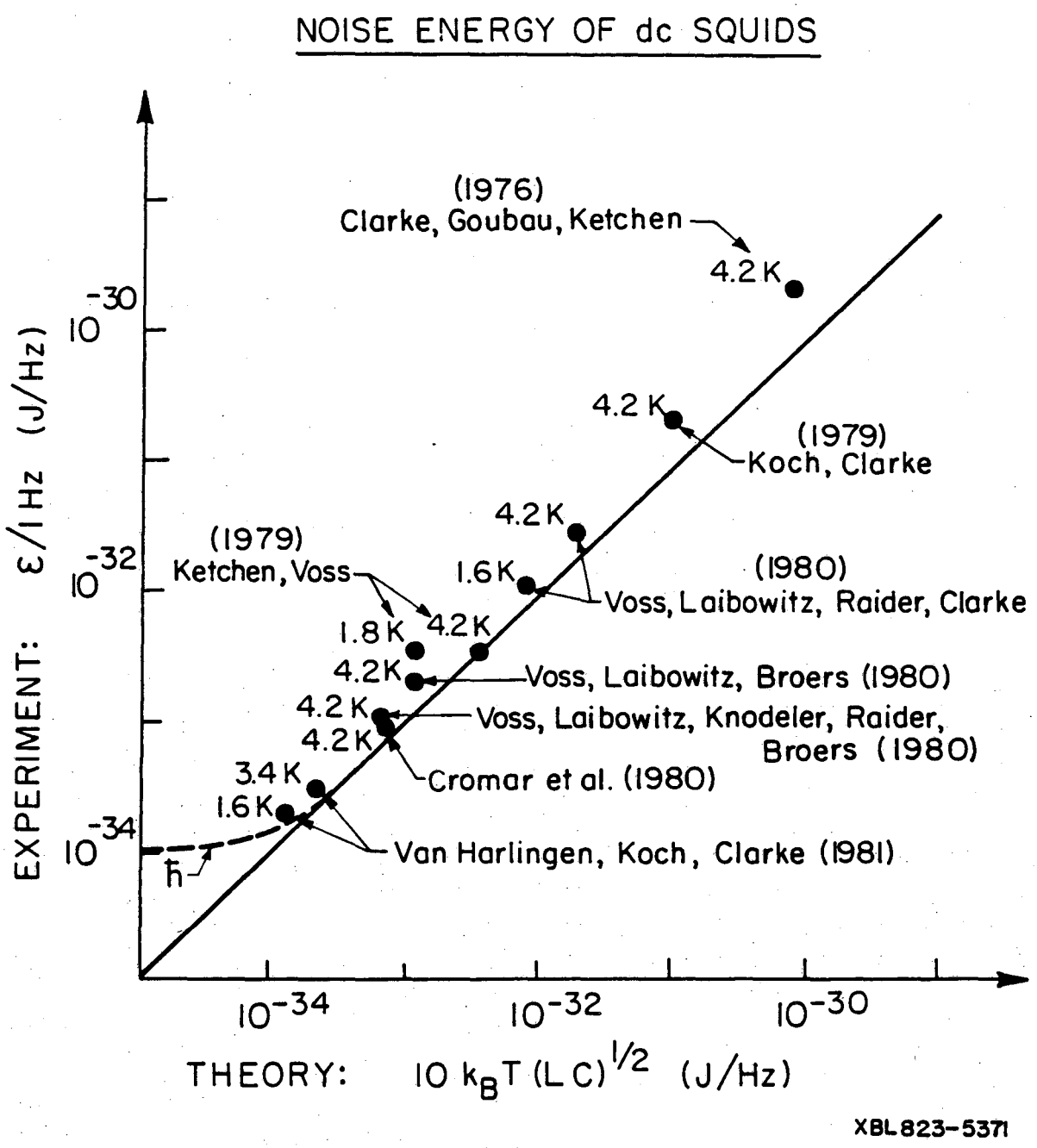

Fig. 1.1 Predicted noise energy vs. measurement for seven tunnel junction dc SQUIDS.

tion as its commonly called, is defined as the smallest amount of signal energy which when applied to the bare SQUID (from a high impedence source so there is no back-action), produces at the SQUID output a signal which just equals the SQUID's own noise in a unit bandwidth, i.e. the signal for which the signal to noise ratio equals one. Chapter IV presents the quantum limited dc SQUID theory; basically putting quantum noise in the RSJ model of the SQUID. Appendix B analyzes the corrections when the SQUID is tightly coupled to an input coil.

Chapter V presents the results of measurements of dc SQUIDs near the quantum limit that were performed primarily by Dale Van Harlingen. These measurements confirmed in part the predictions for the minimum noise energy although no measurements were made of the total equivalent noise power with the SQUID configured as an amplifier. That is very much harder.

When doesn't the RSJ model work?? Recently, measurements by Voss and Webb (1981) and Jackel et al (1981) have shown behavior predicted, in part, by Ivanchenko and Zil'berman (1969) and Caldeira and Leggett (1981) that clearly lies outside the range of validity of the simple RSJ model. (We need the enhanced RSJ). The effect is called Macroscopic Quantum Tunnelling (MQT). The equations of motion predicted by the RSJ model are identical to these of a point-like particle moving down a one dimensional potential (the washboard potential), and the question raised is whether the point-like particle in this model really should be visualized as a small wave packet. If "it's" really a wave packet then one might expect tunnelling to occur if the potential can be made to have metastable wells separated by barriers. This is the

case when $I < I_0$, as was observed by the two above-mentioned measurements.

Is the RSJ model dead?? Yes, in some limits, particularly below the critical current, $I < I_0$; but there exist many measurements when $I > I_0$ that verify it nicely. The question to ask is how wide is the visualized wave packet when compared to the characteristic distance over which the one-dimensional potential changes. If the wave packet is narrow when compared to the potential characteristic width, we have the "particle-like limit" and, using Eherfest's theorems, one has identical equations of evolution for the wave-packet and a point-particle. The key contribution of Appendix C is to show that the well-known transfer Hamiltonian starting model shows conclusively that the wave packet is the correct visualization. After the shunt resistor is added, the Schrodinger equation for the total system becomes non-linear in the wave function, $\Psi(x)$, and stochastic. This stochasticity is the noise we measured. When integrating this equation to follow the evolution of the wave packet, the non-linearity eliminates the common diffusion-like solution for a unbound particle, and forces the wave function to stay compact over arbitrarily long times, like a soliton. This is why the RSJ model works when it does. On the other hand, in the limit of small I_0C, (C is the junction self-capacitance) the diffusion forces overcome the contracting forces and the wave function will spread out everywhere, the "wave-like limit", where MQT was observed.

II. SINGLE JUNCTION THEORY

The effects of thermal noise on a resistively shunted (Stewart, 68; McCumber, 68) Josephson (1962) junction (RSJ) have been extensively studied. The theories assume that the noise originates as Nyquist noise in the shunt resistor R. The junction is modeled as a particle moving in a tilted periodic potential, and the effect of the noise current is to induce random fluctuations in the angle of tilt. These fluctuations have two effects. First, they enable the phase of the junction to slip by 2π when the bias current, I, is less than the noise-free critical current, I_o, thereby producing a voltage pulse across the junction. This effect produces noise rounding of the I-V characteristics at low voltages, V; the noise rounding has been calculated by Ambegoakar and Halperin (1969) and Vystavkin et al. (1974) for the case C = 0 (C is the capacitance of the junction). Subsequently, Kurkijarvi and Ambegoakar (1970) and Voss (1981) computed the case $C \neq 0$. Second, the fluctuations generate a voltage noise when the junction is current biased at a non-zero voltage. Likharev and Semenov (1972) and Vystavkin et al. (1974) showed that for the C = 0 case in the limit $h\nu_J < k_BT$ ($\nu_J = 2e\bar{V}/h$ is the Josephson frequency) and for frequencies much less than ν_J, the spectral density of the voltage noise is given by

$$S_V(0) = \frac{4k_BTR_D^2}{R}\left[1 + \frac{1}{2}\left(\frac{I_o}{\bar{I}}\right)^2\right]. \tag{2.1}$$

Here, R_D is the dynamic resistance. This result was derived on the assumption that the noise is sufficiently small that one can neglect departures of the I-V characteristic from that of the ideal RSJ,

$$\bar{V} = R\left(I^2 - I_o^2\right)^{1/2} . \qquad (2.2)$$

Thus, Eq. (2.1) is not valid in the noise-rounded region $I < I_o$. Voss (1981) and Koch (unpublished) computed the noise for the case $C \neq 0$. Experimental results are in good agreement with calculations for both the noise rounding (Falco et al, 74) and voltage noise (Soulen et al, 78).

For a junction voltage-biased on self-resonant step, Stephen (1969) has calculated the contribution of pair current fluctuations to the linewidth of the Josephson radiation. This noise arises from photon number fluctuations (including zero point fluctuations) in the lossy cavity formed by the junction, and is not intrinsic to the tunneling of Cooper pairs in a non-resonant junction. Experimental results (Dahm, et al, 69) are in good agreement with the predictions.

1. The Equations of Motion and the Washboard Model

We consider a Josephson tunnel junction with critical current I_o and capacitance C shunted with resistance R. We assume that V always lies below $2\Delta/e$, where Δ is the energy gap, so that the Riedel singularity is unimportant. Furthermore, we take the temperature T to be well below the transition temperature, where the quasiparticle tunneling current is small compared with the current in the shunt resistance, so that we can neglect noise from the quasiparticle tunneling current

(Dahm, et al, 69). The only significant noise source is the current noise, $I_N(t)$, in the resistor, which has a spectral density, including zero-point fluctuations, (Callen & Walton, 51)

$$S_I(\nu) = (2h\nu/R) \coth (h\nu/2k_BT) \tag{2.3}$$

at angular frequency ν. We compute the spectral density of the voltage noise, $S_V(\nu)$, for a current-biased RSJ at a frequency ν.

The circuit as constructed is shown in Fig. 2.1(a). Using Kirchhoffs laws and the ac and dc Josephson equations we find the equations of motion for the system:

$$I = C\dot{V} + I_o \sin \delta + V/R + I_N(t) \tag{2.4}$$

and

$$V = (\Phi_o/2\pi)\dot{\delta}, \tag{2.5}$$

Where δ is the phase difference between the two superconducting wave functions across the tunnel barrier. Equations (2.4) and (2.5) can be rewritten as a single equation (letting $I_N(t)=0$ for the time being);

$$\left(\frac{\Phi_o}{2\pi}\right)^2 \left[C\ddot{\delta} + \dot{\delta}/R\right] = \frac{I\Phi_o}{2\pi} - \frac{I_o\Phi_o}{2\pi} \sin \delta = \frac{-dU(\delta)}{d\delta} \tag{2.6}$$

This equation is like the equation of motion of a particle with mass proportional to C, and a viscous damping proportional to 1/R in a one dimensional potential, the washboard potential (Fulton, 75). The analytical form of this potential is:

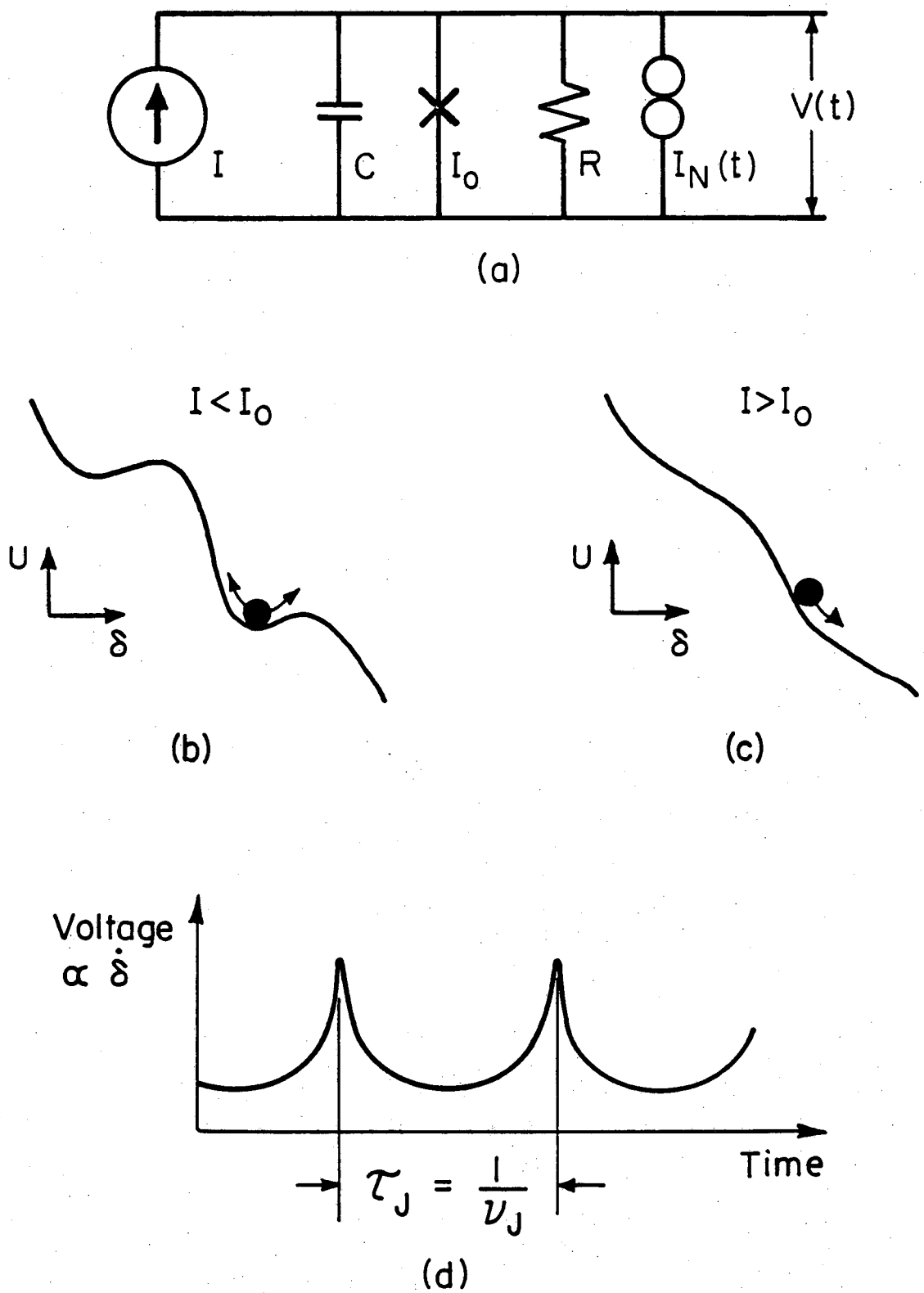

XBL824-5536

Fig. 2.1 (a) Circuit diagram, (b) washboard potential $I<I_o$, (c) washboard potential $I<I_o$, (d) voltage across junction vs. time for I I_o.

$$U(\delta) = -\frac{I\Phi_o}{2\pi}\delta - \frac{I_o\Phi_o}{2\pi}\cos\delta \ . \tag{2.7}$$

The position of the particle in the potential is the junction phase and the voltage across the junction, which varies as $\dot{\delta}$, is just the velocity in the potential.

The potential has two limiting forms: (1) when $I < I_o$ there exist metastable wells (Fig. 2.1(b)) where the particle can be locally stable, and (2) when $I > I_o$ the particle spends its time sliding down the never-ending slope (Fig. 2.1(c)), in a limit cycle whose average cycle time is called the Josepheson time, τ_J, (Fig. 2.1(d)). The inverse of the Josephson time is the Josephson frequency ν_J. Notice the voltage versus time plotted in Fig. 2.1(d) is very non-linear.

The effect of $I_N(t)$ can be quickly seen by observing in Eq. (2.7) that the average slope of the potential is controlled by the bias current. The instantaneous current the junction sees, in the RSJ model, is the sum of the external bias current, I, and the noise current, $I_N(t)$. Hence the slope of the potential will fluctuate around the average value with a power spectrum given by $S_I(\nu)$. When $I > I_o$ the slope fluctuations will cause the time of passage through each limit cycle to vary slightly, i.e. the instantaneous Josephson frequency will fluctuate. Because the limit cycle is extremely non-linear, the average voltage per cycle will also fluctuate, and this means low frequency noise. Current noise in the resistor that produces fluctuations in the potential slope at or near the Josephson frequency will be mixed down to near dc by this non-

linearity. This mechanism allows us to measure noise at many Gegahertz with simple audio frequency equipment if we understand the junction dynamics. The junction acts as a mixer.

In the other limit of the potential, when $I < Io$, the passage of the particle from one well to another can occur in two ways. Noise from the resistor can momentarily reduce the barrier height to zero, allowing the particle to escape. The noise can be thermal or quantum noise from the resistor giving rise to the terms "thermal" or "quantum activation." The activation process is appropriate in the particle-like limit, but in the wave-like limit, when the width of the wave function of the particle is large compared to the characteristic width over which the potential changes, the particle may also tunnel through the barrier (Ivanchenko and Zil'berman, 69).

It is convenient to introduce the dimensionless units and parameters, $\omega = 2\pi\nu$, $i=I/I_o$, $v=V/I_oR=\omega_J/(2\pi I_oR/\Phi_o)$, $\Gamma = 2\pi k_BT/I_o\Phi_o$, $\theta = \omega/(2\pi I_oR/\Phi_o)$, $S_i(\theta) = S_I(\omega)(2\pi R/I_o\Phi_o)$, $S_v(\theta) = S_V(\omega)(2\pi/I_o\Phi_oR)$, $\beta_c \equiv 2\pi I_oR^2C/\Phi_o$, and $\kappa \equiv eI_oR/k_BT$.

2. Analytical Solutions of the Equations when $I > I_o$

We calculate the properties of the RSJ from the instantaneous phase difference across the junction, $\delta(t)$, which evolves in dimensionless time $t/(\Phi_o/2\pi I_oR)$ according to the Langevin equation

$$\beta_c \ddot{\delta} + \dot{\delta} + \sin\delta = i + i_N \quad . \tag{2.8}$$

The use of a noise term which includes quantum fluctuations, Eq. 2.3, in the classical equation, Eq. 2.8, yields the noise charac-

teristics of the junction in all regimes from the thermal to the quantum limit if the junction is in the particle limit.

We first consider the limit $\beta_c << 1$ in which the term $\beta_c\ddot{\delta}$ may be neglected in Eq. 2.8. (As $\beta_c \to 0$, the roll-off frequency of the noise, $\sim 1/RC$, increases, and the mean square current noise available to the junction, $\propto (1/RC)^2$, eventually becomes so large that the noise-rounded critical current is reduced to zero. In the analytical discussion we choose $0 < \beta_c << 1$, while for the computer results we choose $\beta_c \simeq 0.1$.) In the limit in which noise-rounding effects are negligible ($i>1$), the I-V characteristic is $v = (i^2-1)^{1/2}$ and Eq. 2.8 may be solved analytically using the Likharev and Semenov (1974) (LS) method. One calculates the Fourier components of the voltage fluctuations taking into account the mixing down of high frequency noise at harmonics of the Josephson frequency and finds the spectral density

$$S_v(\theta) = \sum_{k=-\infty}^{\infty} |z_k|^2 \, S_i(\theta - kv). \tag{2.9}$$

Here, k is an integer, and

$$|z_k| = \left| \delta_{k,o} + \frac{ki(i-v)^{|k|}}{\theta - kv} - \frac{1}{2}\left[\frac{(k-1)(i-v)^{|k-1|}}{\theta - (k-1)v} + \frac{(k+1)(i-v)^{|k+1|}}{\theta - (k+1)v}\right]\right| \tag{2.10}$$

Evaluating the z_k in the limit $\theta/v \to 0$, that is, when the measurement frequency is much lower than the Josephson frequency, we find

$$S_v(0) = \left[i^2 S_i(0) + S_i(v)/2\right] v^{-2} + 0\left[\frac{\theta^2}{v^2} \sum_{k\geqslant 2}^{\infty} \frac{S_i(-kv)}{k^4}\right] \quad (\theta << v) \qquad (2.11)$$

Even in the extreme quantum limit in which $S_i \sim kv$, the sum still converges, so that the last term is of order θ^2/v, which is negligible in the limit $\theta \ll v$.

Substituting Eq. 2.3 into Eq. 2.11 we find the result, valid for $i>1$,

$$S_v(0) = \frac{2\Gamma r_D^{\,2}}{\pi}\left[1 + (\kappa v/2i^2)\coth(\kappa v)\right] , \qquad (2.12)$$

where $R_D = \partial v/\partial i = i/v$, or, in dimensioned units,

$$S_V(0) = R_D^{\,2}\left[\frac{4k_BT}{R} + \frac{2eV}{R}\left(\frac{I_o}{I}\right)^2 \coth\left(\frac{eV}{k_BT}\right)\right] , \qquad (2.13)$$

where $R_D = \partial V/\partial I$ is the dynamic resistance. This equation is plotted in Fig. 2.2. The inset of Fig. 2.2 shows the temperature dependence of $S_V(0)$ for particular values of I_o (assumed to be independent of temperature) and R at fixed bias current. For comparison, the LS result in the classical limit is also shown.

The physical meaning behind the two terms in Eq. (2.13) is easy to understand. The first term in square brackets, $\Delta k_BT/R$ represents the current noise in the resistor starting out at the measurement frequency, which is low enough to see the junction and bias supply as a simple

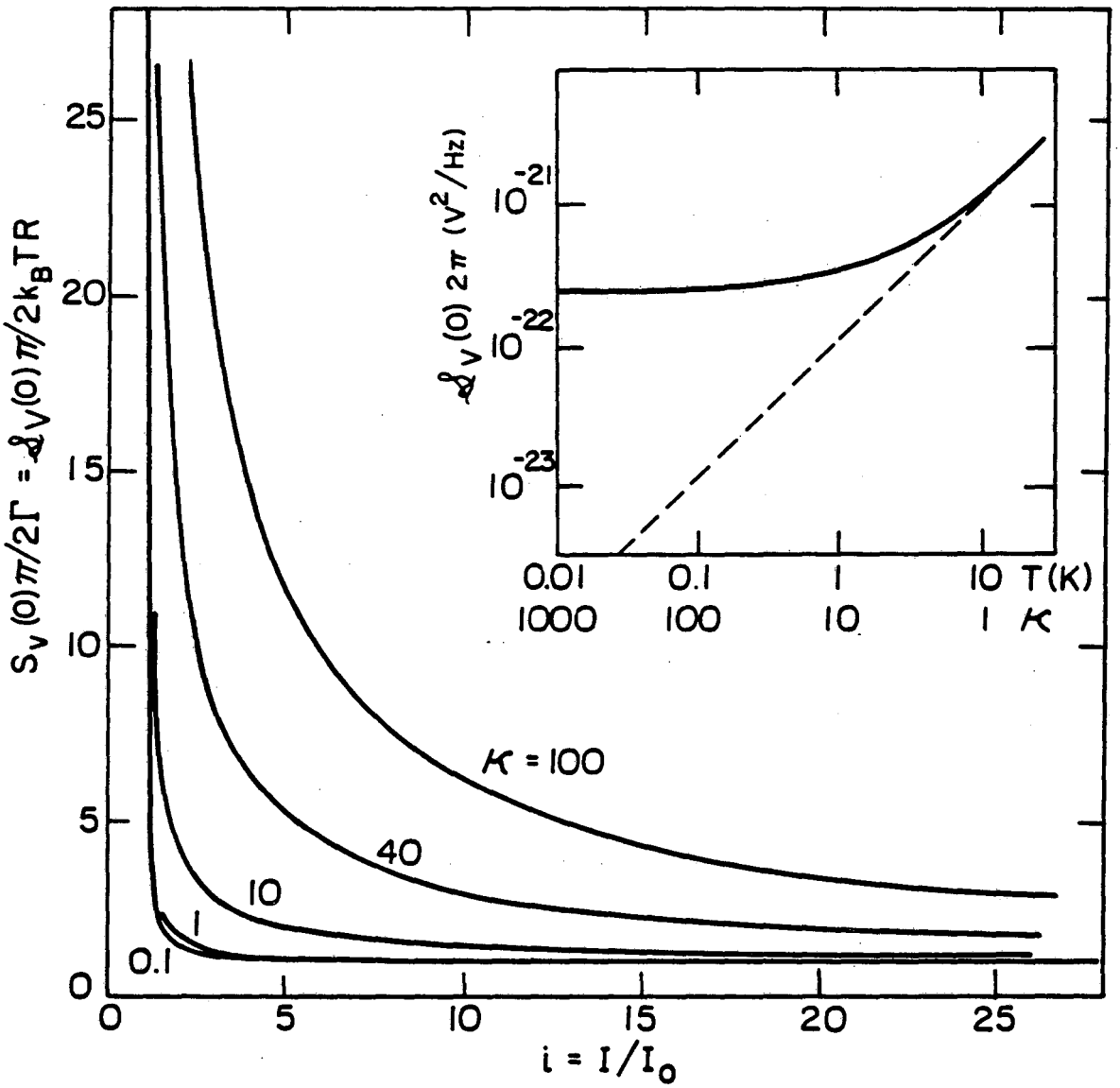

XBL 804-5062

Fig. 2.2 Low frequency spectral density $S_V(0)$ of the voltage noise vs. current for 5 values of $\kappa \equiv eI_oR/k_BT$ with $\beta_c \ll 1$. Inset shows $S_V(0)$ vs. T for I_o = 1mA, I = 1.41mA, and R = 0.86Ω (chosen to give $V = I_oR$ and $\kappa \equiv 10$ at 1K). Dashed line shows the LS classical result. Dimensionless power spectral density are per dimensionless hertz.

resistor of value R_D. The resulting output voltage noise is just R_D^2 times the input noise, no mixing occurs. The second term is a product of the current noise at the Josephson frequency, $(4eV/R)\coth(eV/k_BT)$, times a mixing coefficient, $(R_D I_o/I)^2/2$. The mixing coefficient tells us how well the non-linearity of the junction's phase evolution mixes noise starting out at the Josephson frequency down to the much lower measurement frequency.

It is instructive to consider several limits of Eq. (2.13): (i) $eV \ll k_BT$ ($\kappa v \ll 1$): We obtain the LS result $S_v(0) = \Delta k_B T R_o^2/R \quad [1+(I_o/I)^2/2]$. (ii) $eV \gg k_BT$ ($\kappa v \gg 1$): We obtain $S_V(0) = R_D^2\,[4k_BT/R + 2eVI_o^2/(RI^2)]$ For $eV \ll k_BT(I/I_o)^2$ ($vr_D^2 \gg \kappa$) this yields the Nyquist result $S_V(0) = 4k_BTR$, while for $eV \gg k_BT(I/I_o)^2$ ($vr_D^2 \ll \kappa$) we find the quantum limit

$$S_V(0) = 2eV(I_o/I)^2 R_D^2/R = 2eI_o^2R^3/V. \tag{2.14}$$

Thus, to observe quantum effects we require $\kappa \equiv eI_oR/k_BT \gg 1$. At the particular bias $V=I_oR$, Eq. (2.14) reduces to $S_V(0) = 2eI_oR^2$, which is just the voltage spectral density of the shot noise due to a current I_o flowing through a resistance R. However, it should be clear from the derivation that Eq. (2.14) arises not from an intrinsic shot noise in the pairs tunneling through the barrier but rather from the zero-point fluctuations of the shunt resistance which have a current spectral density $2h\nu/R$.

3. Computer Solutions

To compute the noise rounding of the I-V characteristics or to include the effects of a non-zero capacitance, we have used numerical

techniques. Although we have computed the general case $T \neq 0$, we report here results only for the $T=0$ limit in which Eq. (2.3) becomes $2h\nu/R$. We used an LSI-11 computer to integrate Eq. (2.8) using a noise driving term obtained by digitally filtering pseudo-random white noise. We obtained the mean voltage by averaging the instantaneous voltage over typically 10^4 Josephson cycles, and determined the low frequency spectral density of the voltage noise by averaging the fluctuations in the voltage after low-pass digital filtering (see Appendix A for more on the computer methods). The accuracies of the average voltage and the spectral density are believed to be $\pm 5\%$ and $\pm 10\%$ for $i>1$, and $\pm 10\%$ and $\pm 20\%$ for $i \leq 1$. Figure 2.3 illustrates the noise rounding of the I-V characteristics due to zero point fluctuations for $\beta_c \approx 0.1$. For a given depression of the critical current below the noise-free value, the rounding extends to much larger values of voltage than in the equivalent thermal noise case (Ambegoakar and Halperin, 69) because the noise in the resistor at the Josephson frequency increases with voltage.

In these computer solutions we have not included in our calculation the possibility of macroscopic quantum tunneling. The tunnelling rate including the effect of dissipation (Caldeira and Leggett, 81) at $T=0$ is predicted to be:

$$R_{M.Q.T.} = B \exp\left\{ - \left(7.2 + 8A/\left[\beta_c^{1/2}(1-i^2)^{1/4}\right]\right) \Delta U(i)/\hbar\omega_o \right\}. \tag{2.15}$$

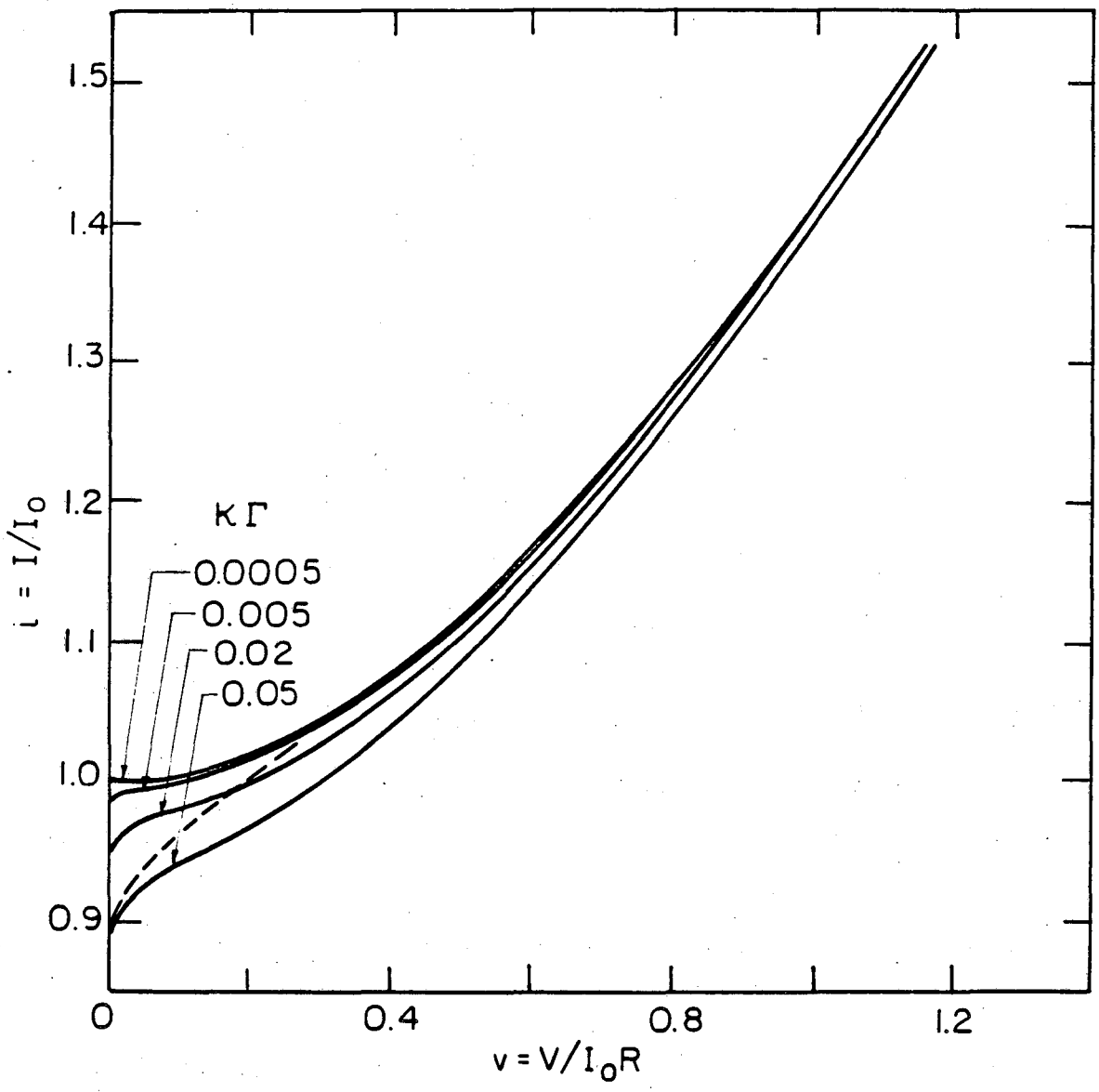

XBL 807-5556

Fig. 2.3 I-V characteristics at T = 0 with $\beta_c \approx 0.1$ for 4 values of $\kappa\Gamma \equiv 2\pi eR/\Phi_0$, showing rounding due to zero-point fluctuations. Dashed line shows noise rounding in the thermal noise limit for a similar depression in critical current as for the case $\kappa\Gamma = 0.05$.

Where B is an exponential prefactor, A is a factor on the order of 1, and ω_o is the natural frequency of the particle in the well; $\omega_o = (2\pi I_o/\Phi_o C)^{1/2} (1-i^2)^{1/4}$. As β_c gets small the MQT rate drops according to the formula, intuitively because the wave function is contracted by the dissipation. Eventually the junction will be in the particle-like limit.

The barrier passage rate at T=0 from quantum activation for β_c=0.3 has been calculated to be:

$$R_{Q.A.} = B \exp \left\{ - (0(10)\ \Delta U(i)/\hbar\omega_o) \right\} . \qquad (2.16)$$

The calculations were done using the classical Langevin equation with a quantum driving term, so they are only accurate in the particle-like limit. However as $\beta_c \to 0$ the junction will be in the particle like limit, and the MQT rate will fall below the quantum activation rate, which will validate the classical Langevin approach.

For this reason as $\beta_c \to 0$ the quantum noise rounding predictions plotted in Fig. 2.3 and the dc SQUID calculation in Section IV are valid (the SQUID performance always peaks just in the beginning of the noise rounded region).

Figure 2.4 shows the effects of increasing β_c. The dynamic resistance increases markedly at low voltages Fig. 2.4(a) as β_c increases; hysteresis occurs for $\beta_c \geqslant 1$. Figure 2.4(b) shows the corresponding spectral densities of the voltage noise, with the dotted line taken from Eq. (2.13). For v>0.5 the noise rounding is small, and the computer and analytical results are indistinguishable. The increase in noise with increasing β_c for a given voltage at low voltages reflects

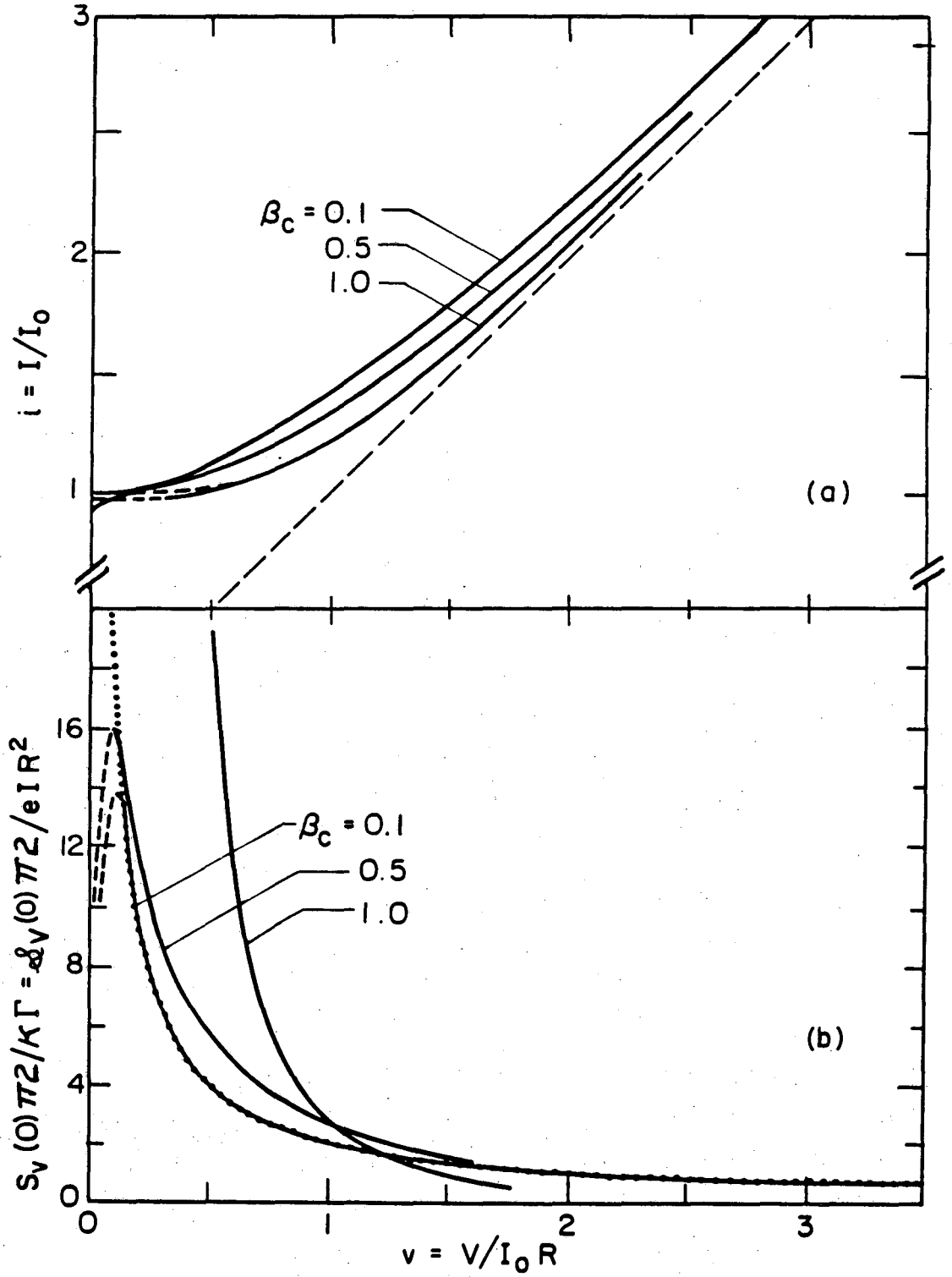

XBL804-5061

Fig. 2.4 (a) I-V characteristics at T = 0 for $\kappa\Gamma = 2\pi eR/\Phi_o$ = 0.0194 (R=40Ω) with $\beta_c \approx 0.1$, = 0.5, 1. (b) Spectral density of the voltage noise for the curves in (a); dotted line is taken from Eq. (2.12). The dashed portions are of lower accuracy. Dimensionless power spectral density are per dimensionless hertz.

the higher dynamic resistance, but for all β_c at very low voltages the noise decreases with decreasing voltage because of noise rounding. At high voltages, the noise decreases with increasing β_c at a given voltage because the noise currents are filtered out at frequencies above $\sim 1/RC$.

4. Concluding Remarks

In conclusion, we note that the quantum effects calculated here should be observable provided one can obtain the limit $\kappa >> 1$. Writing $\kappa = (e/k_B T)(\beta_c \Phi_o j_1/2\pi c)^{1/2}$, where j_1 is the critical current density and c is the capacitance per unit area of the tunnel junction, we see that the limit requires a high current density and/or a low temperature. At 1K, with $j_1 = 10^4 \mathrm{Acm}^{-2}$, $\beta_c = 1$ and $c = 0.04\ \mathrm{pF\mu m}^{-2}$, we find $\kappa = 10$, a value at which quantum corrections are considerable (see inset of Fig. 2.2). Our results for $\beta_c << 1$ should also be applicable to point contact junctions and micro-bridges to the extent that these devices can be represented by the RSJ model.

III. SINGLE JUNCTION MEASUREMENTS

In order to test the theory of Section II, measurements were made of the low frequency spectral density of the voltage noise, $S_v(0)$, in current-biased resistively shunted Josephson tunnel junctions under conditions in which the noise mixed down from frequencies near the Josephson frequency (ν_J) to the measurement frequency ($\ll\nu_J$) is in the regime $h\nu_J > k_BT$. In this limit, quantum corrections to the mixed-down noise are important. The values of $S_v(0)$ measured on junctions with current-voltage (I-V) characteristics close to the predictions of the Stewart-McCumber model were in excellent agreement with the prediction for $I > I_o$, $S_v(0)/R_D^2 = (4k_BT/R) + (2eV/R)(I_o/I)^2\coth(eV/k_BT)$, with no fitted parameters. Here, R and R_D are the shunt and dynamic resistance, and I_o is the critical current in the absence of noise. In particular, the mixed-down noise at voltages above 300 μV did not change significantly when the temperature was lowered from 4.2K to 1.6K, and was in excellent agreement with the prediction $(2eV/R)(I_o/I)^2$ that is valid when $h\nu_J > k_BT$. This result demonstrates that the limiting noise arises from zero-point fluctuations in the shunt resistor. The mixed-down noise for a wide range of bias voltages was used to compute the spectral density of the current noise in the shunt resistor, $S_I(\nu)$, at frequency ν. With no fitted parameters, the measured value of $S_I(\nu)$ at frequencies up to 500 GHz was in excellent agreement with the Callen-Welton (1951) prediction $(2h\nu/R)\coth(h\nu/2k_BT)$ at 1.6K and 4.2K. The presence of the zero-point term, $2h\nu/R$, where $h\nu > k_BT$ was clearly shown. The I-V curves of a junction with $\beta_L \equiv 2\pi I_o L_s/\Phi_o \sim 0.5$ and $\beta_c \equiv 2\pi I_o R^2 C/\Phi_o \ll 1$, where C is the junction

capacitance and L_s is the shunt loop inductance, showed structure at voltages where the Josephson frequency was near a subharmonic of the L_sC resonant frequency. The additional non-linearity of the I-V characteristic caused mixing down of noise near higher harmonics of the Josephson frequency, thereby greatly enhancing the measured voltage noise. The measured spectral density of the noise was in good agreement with that of a computer simulation in which the values of L_s and C were fitted to match the measured I-V characteristic. These data also clearly demonstrated the quantum corrections to the mixed-down noise, and, in particular, the presence of the zero point term.

1. Experimental Procedures

A. Junction Fabrication

To observe quantum noise effects, we require junctions with $\kappa \gtrsim 1$. Writing $\kappa = (e/k_BT)(\beta_c\Phi_o j_1/2\pi c)^{1/2}$, where j_1 is the critical current density and c is the capacitance per unit area, we see that junctions with high critical current densities are necessary to observe these effects in the liquid He^4 temperature range. At 4.2K, with $\beta_c = 0.2$, $j_1 = 10^4 A\ cm^{-2}$ and $c = 0.04pF\ \mu m^{-2}$ we find $\kappa \approx 1.1$. This is a convenient value of κ, since, as the temperature is lowered to near 1K, κ increases so that quantum effects become dominant.

Our PbIn-In_2O_3-Pb tunnel junctions, resistively shunted with CuAl films, were fabricated on glass substrates using the photolithographic lift-off techniques described by workers at IBM (Greiner, et al, 80). The configuration is shown in Fig. 3.1(a). We first deposited a 10 μm-wide Cu (0-3 wt.% Al) film 40 to 100 nm thick, and then evaporated a 10 μm-wide, 250 nm-thick Pb (10 wt.% In) film at

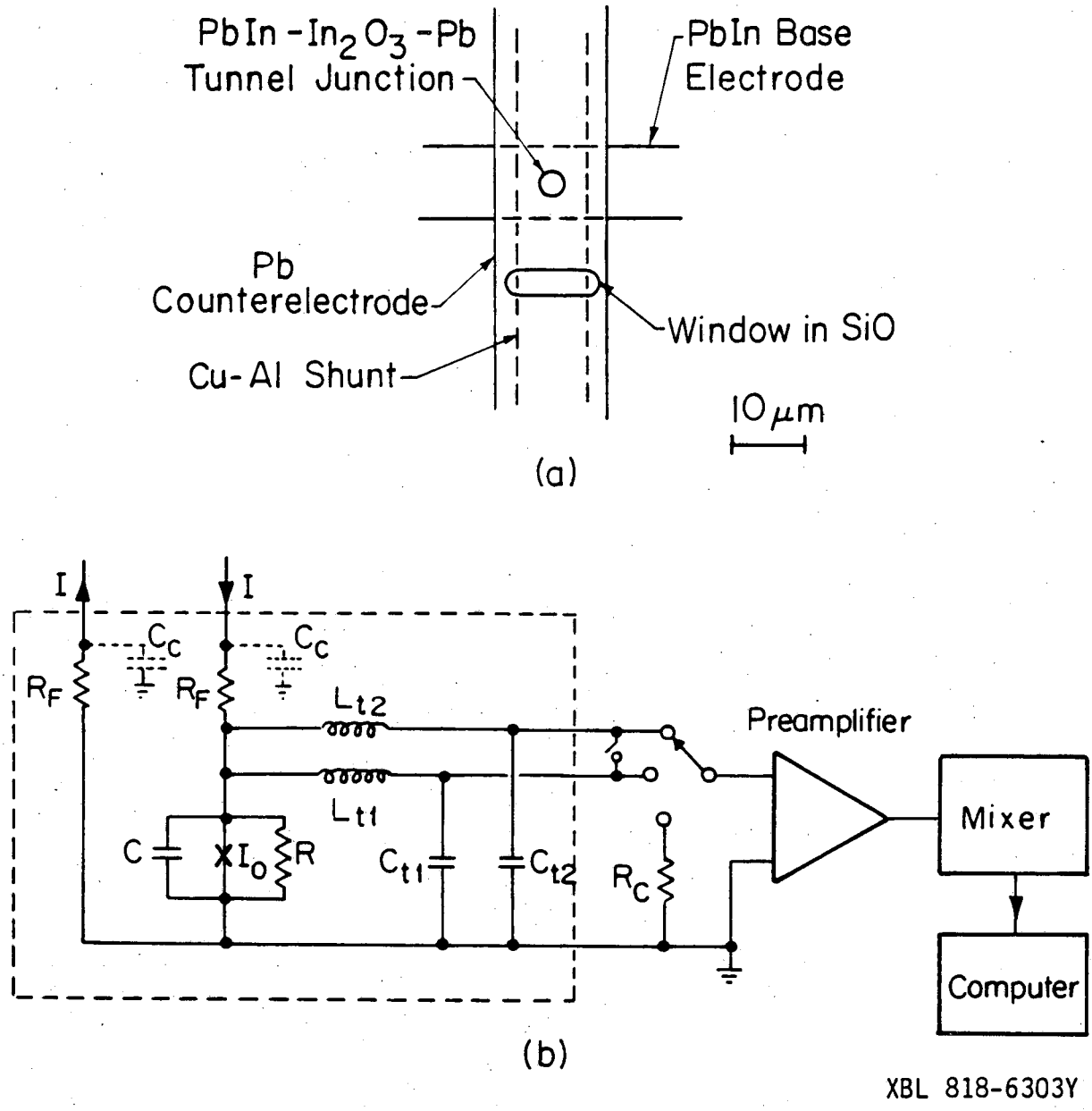

Fig. 3.1 (a) Configuration of resistively shunted tunnel junction; (b) Schematic of measuring circuit; the dashed lines enclose the components immersed in liquid helium.

right angles to the CuAl strip. After another resist patterning, a SiO oxide layer, 100 nm thick, was deposited and two windows were opened by lifting off the SiO to expose the PbIn and CuAl films. After patterning the resist for the upper electrode, the exposed metal surfaces were cleaned by rf sputter-etching in Ar, the In_2O_3 oxide was grown thermally in a low pressure of oxygen, and the 400 nm-thick Pb counter-electrode was deposited and lifted off. A final protective layer of SiO was then evaporated. The diameter of the junction was about 2.5 μm, and the critical current ranged from 0.1 to 2 mA (0.2 to 4×10^4 A cm^{-2}) at 4.2K, depending on the oxidation parameters. The capacitance of the junction was estmated to be 0.5 pF (see Sec. III.2.D). The resistive shunt was about 5 μm long and ranged in resistance from 0.05 to 0.7Ω , depending on the thickness and composition of the CuAl. The Pb counterelectrode formed a ground plane for the shunt, reducing its inductance, L_s, to about 0.2 pH. The critical currents of these junctions proved to be quite reproducible for a given set of oxidation conditions, and the junctions could be recycled between room and liquid helium temperatures at least several times without significant deterioration. We found that storing the junctions at room temperature for (say) 24 hours caused their critical currents to decrease (up to a factor of 2), while annealing them at 70°C for (say) 1 hour caused their critical currents to increase. Thus, if necessary, we could adjust the critical current somewhat, as we did with junction 3. Leads were attached to the junctions with pressed In pellets.

Junctions fabricated with these techniques omitting the resistive shunts displayed excellent tunneling characteristics with little excess current at voltages below the sum of the gaps.

B. Measurement Procedures

Before measuring the noise of a given junction, we plotted its I-V characteristic and dynamic resistance on a X-Y recorder, thus determining its critical current and the presence of any resonant structure. By applying an external magnetic field or by trapping the critical current to near zero we obtained the shunt resistance.

The noise measurement procedures now to be described were those that we used in the later measurements where most of the data were collected. Small modifications to the procedures used in the earlier work will be mentioned at the appropriate places in Sec. III.2. The circuit for measuring the noise across a junction is shown in Fig. 3.1(b). The bias current was filtered by two low-pass filters each consisting of a cooled 1.5 kΩ resistor, R_F, and the cable capacitance, C_c. The junction was connected across two cooled LC-resonant circuits with inductors L_{t1}, L_{t2} and capacitors C_{t1}, C_{t2} (in fact, four-terminal connections were used). In a typical experiment, L_{t1} = 69 μH, L_{t2} = 35 μH, C_{t1} = 75 nF, and C_{t2} = 21.5 nF, giving resonant frequencies of 70 and 183 kHz. The leads across each tank circuit were connected in turn to a Brookdeal 5004 preamplifier to measure the noise across the junction at the appropriate frequency. In addition, by connecting together the leads across the tank circuits at the top of the cryostat we could measure the noise at a third, intermediate frequency, about 106 kHz for the values given above. After further

amplification, the noise from the preamplifier was mixed down to frequencies below 500 Hz using a PAR 124. After low-pass filtering, the spectral density of the noise was measured using a PDP-11 computer. The junction, which was immersed directly in liquid He^4, was enclosed in a lead can, and the cryostat was surrounded by a mu-metal shield. The cryostat, bias supply, and preamplifier were enclosed in a shielded room.

To make the noise measurements, we first adjusted the bias current through the junction to obtain the required voltage, which was measured with a high-impedance voltmeter. We measured the voltage noise with the appropriate resonant circuit, using a typical averaging time of 10 min. The noise produced by the junction across the tank circuit was $Q^2 S_v(0) = \omega^2 L_t^2 \, S_v(0)/R_d^2$, so that the required quantity $S_v(0)/R_D^2$ was independent of Q. We note that the predicted value os $S_v(0)/R_D^2$ is virtually independent of β_c in the range $0 < \beta_c < 0.5$, while the value of $S_v(0)$ does increase significantly as β_c is increased in this range (Voss, 81). Thus, for β_c appreciably greater than zero (junctions 2 and 3), it is much more reasonable to compare experimental and theoretical values of $S_v(0)/R_D^2$, rather than values of $S_v(0)$. However, a knowledge of the tank circuit impedance, $Q^2 R_D$, was required to enable us to subtract the preamplifier current noise. We determined Q at each bias point by exciting the tank circuit inductively and measuring the half-power frequencies, using a function generator. From time to time during the noise measurements, the gain of the preamplifier-mixer-computer chain was calibrated by measuring the Nyquist noise across a room-temperature resistor R_c (5.1 kΩ) connected to the input

of the preamplifier. We estimate the accuracy of the gain to be $\pm 2\%$. These measurements of the noise and of Q were repeated at each of the three frequencies for a series of voltages at each temperature and for a range of temperatures. Below 4.2K, the temperature of the helium bath was controlled by regulating the vapor pressure.

We now discuss the various measured corrections to the noise:

(i) The spectral densities of the voltage noise contributed by the preamplifier voltage noise (typically 6.1×10^{-19} V^2Hz^{-1} at 183 kHz) and current noise (typically 2.8×10^{-26} A^2Hz^{-1} at 183 kHz) were subtracted from the measured spectral density. The spectral density of the current noise was measured in a separate experiment by measuring the voltage noise across a cooled LC-resonant circuit containing a known resistor. The spectral density of the voltage noise was obtained during each set of measurements on a junction by shorting the input of the preamplifier. Because the current noise was checked less frequently than the voltage noise, we designed the tank circuits so that the contribution of the former was typically 25% of the latter. The total preamplifier noise was comparable with the junction noise at 4.2K, and as much as three times higher than the junction noise at 1.6K; the corresponding errors introduced by the correction varied from $\pm 5\%$ to $\pm 15\%$ of the spectral density of the noise in the junction.

(ii) Losses in the tank circuit (for example, due to the presence of stray resistance) are a source of noise. The spectral density of this contribution was quite negligible (~0.1%) for the 70- and 183-kHz tank circuits. However, the 106-kHz tank circuit contained two leads, parts of which were at room temperature. Their noise con-

tribution was measured with the junction in the zero resistance state, and was typically comparable with the spectral density of the voltage noise of the junction. The error in the correction at 106 kHz was $\pm 5\%$.

(iii) From the noise measurements at the three frequencies and at each bias voltage and temperature we determined that some junctions (2 and 4) generated a small excess noise with a spectral density very close to 1/f. The spectral density was proportional to $(\partial V/\partial I_o)^2$, suggesting that the noise arose from fluctuations in the critical current (Clarke and Hawkins, 76). For example, for junction 2 the 1/f noise at 183 kHz was typically 5% of the spectral density of the voltage noise at the higher bias voltages, where $\partial V/\partial I_o$ became small. We subtracted the measured 1/f noise from the total junction noise at 183 kHz; even if the uncertainty in the noise was as high as 30%, the error introduced was no more than $\pm 3\%$.

(iv) The noise measurements were all performed at bias voltages well below the sum of the gaps of the two superconductors. The quasiparticle current contributes a noise with a current spectral density (Dahm, et al, 69) $2eI_{qp}\coth(eV/2k_BT)$, where I_{qp} is the quasiparticle current. Thus, the ratio of the spectral density of the quasiparticle noise to the predicted spectral density of the mixed-down noise is of order $I_{qp}/(V/R)$, which we estimate to be $\sim 10^{-2}$ at 4.2K over the voltage range of interest. At the lower temperatures, the quasiparticle current is substantially reduced, and its noise contribution is even smaller. Thus, we have neglected quasiparticle noise.

(v) The power dissipation in the shunt resistor caused its temperature to rise significantly above the bath temperature at the higher

bias voltages in some junctions. For each junction we determined the heating effect as a function of temperature by reducing the critical current almost to zero and measuring the Nyquist noise of the shunt as a function of power dissipation. At low bias voltages the measured noise agreed with the Nyquist formula to within $\pm 3\%$. For most junctions the heating effect was important only at bias voltages $V \gg k_B T/e$, where the mixed-down term in Eq. (1.5) is nearly independent of the shunt temperature. Thus, it was sufficient to correct the data by subtracting the increase in the noise generated at the measurement frequency, $4k_B \Delta T/R$, from the measured value of $S_v(0)/R_D^2$, where ΔT is the temperature rise. In these cases, the heating correction was uncertain by $\pm 10\%$ and was at most 30% of the total noise spectral density of the junction, thereby introducing a maximum error of $\pm 3\%$ into the measurement. However, for junction 3, where the heating correction was particularly large, it was necessary to correct the mixed-down term as well by also subtracting $(4h\nu/R)\ \{[\exp(h\nu/k_B T^*)-1]^{-1} - [\exp(h\nu/k_B T)-1]^{-1}\}$ from the data, where $T^* = T + \Delta T$.

(vi) We took considerable care to shield the experiment from extraneous noise sources, and designed the measurement circuitry to avoid coupling significant 300K noise into the low-temperature circuitry. Measured values of the Nyquist noise in cooled resistors in the range 1.5 to 4.2K were within $\pm 3\%$ of the predicted value. Furthermore, measurements on junctions in the classical limit $eV < k_B T$ showed the correct temperature dependence and were in excellent agree- with theory (see Sec. III.2.A). Thus, we believe our measurements were not significantly influenced by extraneous noise sources.

2. Experimental Results and Comparison with Theory

We report results on four different junctions that illustrate various aspects of the theory. The essential parameters of the junctions are listed in Table 3.1.

A. Junction 1

As a test of our measurement system and of the effectiveness of the shielding we first investigated a junction in the limit $\kappa << 1$ in which the Likharev-Semenov (1972) result, Eq. (2.1) is applicable. At 4.2K, the value of κ was 0.066. The parameters β_c and $\beta_L \equiv 2\pi L_s I_o/\Phi_o$ were 0.003 and 0.2, respectively, so that the I-V characteristic was very close to that for an ideal resistively shunted junction (see Sec. III.2.D for a discussion of the effects of the value of β_L). The 1/f and heating corrections were negligible throughout the range of measurement, so that the only corrections to the measured data were for preamplifier and tank circuit noise. (In this experiment, the measurements were at two frequencies only, 30 and 100 kHz.) In Fig. 3.2 we compare the measured noise with the predictions of Eq. (2.1). In plotting the theoretical points we used the predicted dynamic resistance (Stewart, 68; McCumber, 68).

$$R_D = R[1 - I_o^2/I^2]^{-1/2} \tag{3.1}$$

so that only the measured values of R, I_o, I, and T were used. Thus, we have neglected noise rounding, (Ambegoakar and Halprin, 69) and the predicted spectral density of the noise diverges as $I \to I_o$. Above the noise-rounded region, the agreement between theory and experiment

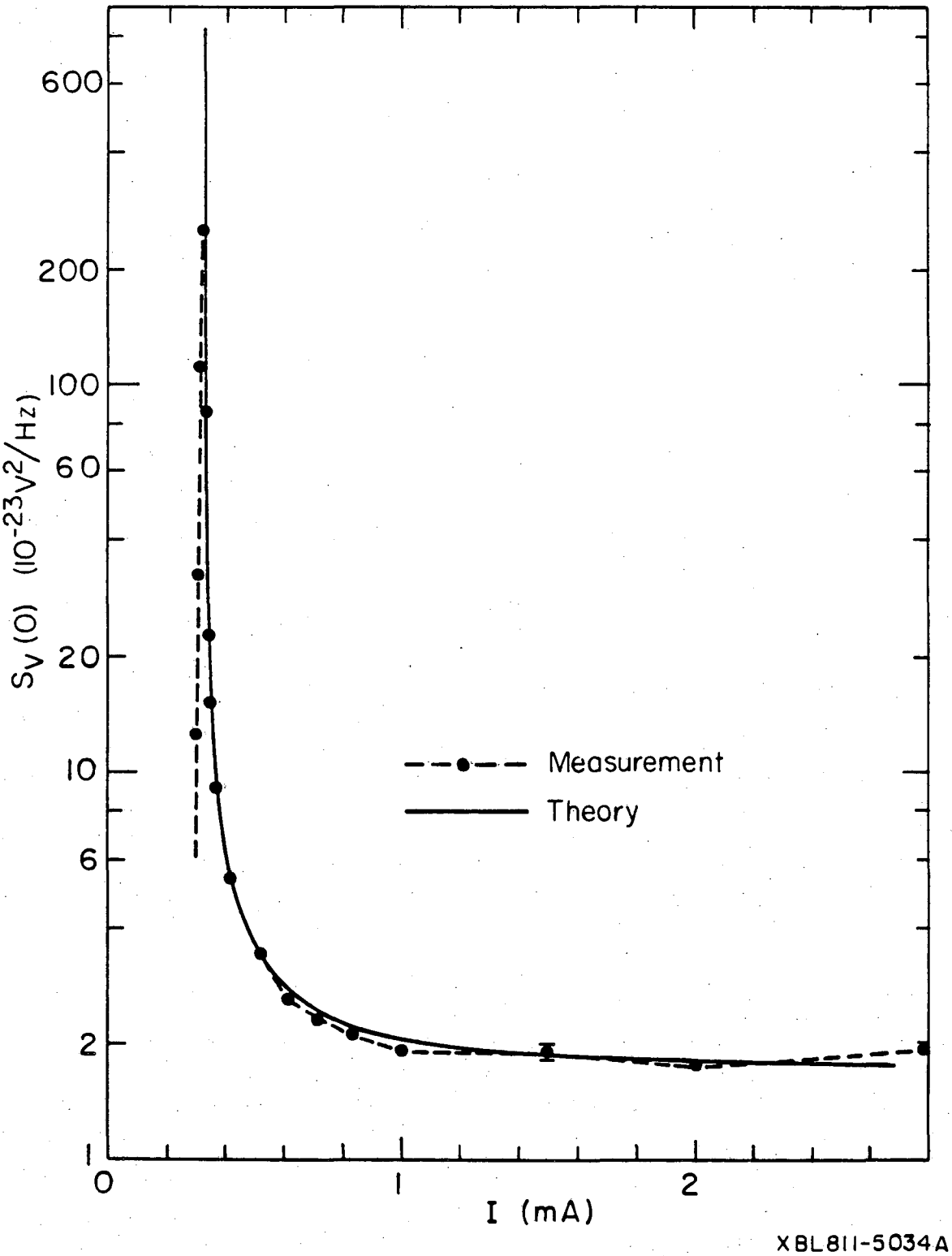

Fig. 3.2 $S_V(0)$ vs. I for junction 1 at 4.2K. Solid circles are data with dashed line drawn through them; solid line is prediction of Eq. (2.1).

is very good indeed. At very low voltages, the measured noise decreases as the current is lowered because the noise-rounded dynamic resistance decreases.

The good agreement between theory and experiment for $I > I_o$ indicates very strongly that the contribution of extraneous noise sources is negligible.

B. Junction 2

The parameters of this junction (Table 3.1) were chosen to emphasize the quantum effects: Thus κ increased from 0.99 at 4.2K to 3.0 at 1.6K (the critical current increased slightly as the temperature was lowered). The values of β_c and β_L, about 0.38 and 0.31 at 4.2K, respectively, were small enough that the deviations from the ideal resistively shunted junction were relatively minor. Figure 3.3 shows I and dV/dI vs. V at 4.2K. There is a small drop in dV/dI at about 800 μV which we believe is associated with a resonance of the shunt inductance and the junction capacitance (see Sec. III.2.D). There is also some very fine structure and a dip at 300 μV of unknown origin. We emphasize that in comparing the quantity $S_v(0)/R_D^2$ with the theory, small deviations in R_D from Eq. (3.1) will be suppressed provided the mixing coefficient $(I_o^2/2I^2)$ in Eq. (2.13) is not affected by the additional non-linearity. Another deviation from the simple model arose because the shunt resistance, R, which was measured with the critical current suppressed nearly to zero, varied between 0.65Ω and 0.75Ω as the voltage bias was increased from 0 to 1 mV. We believe this variation was the result of a proximity effect between the shunt and the electrodes, or possibly of diffusion of Pb into

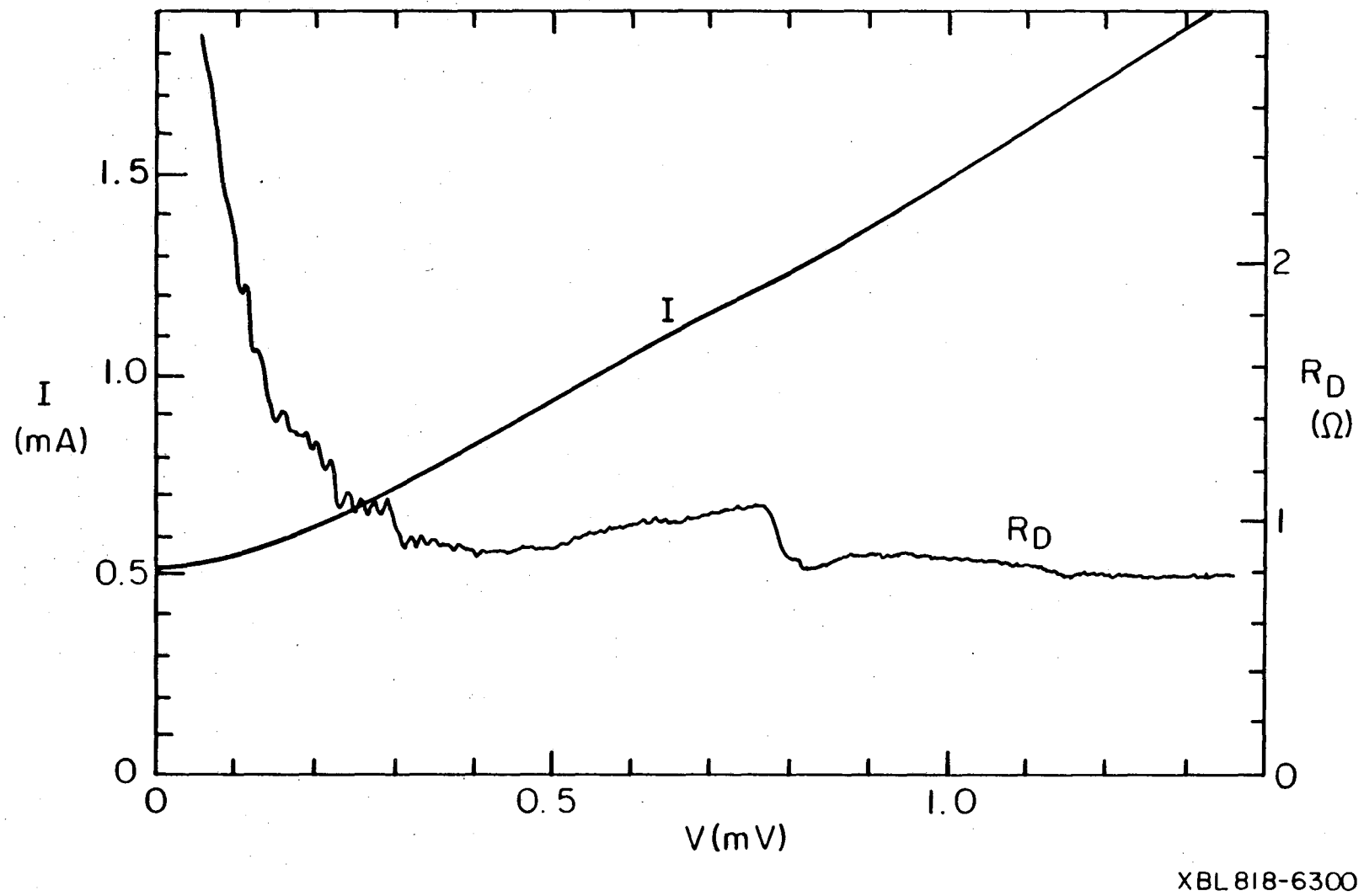

Fig. 3.3 I and R_D vs. V for junction 2 at 4.2K.

the shunt. The measured value of R was used at each voltage bias when we compared theory and experiment.

In Fig. 3.4 we plot measured values of $S_V(0)/R_D^2$ vs. voltage (open circles) after the preamplifier noise has been subtracted. The solid circles are the noise after the 1/f noise subtraction and the heating correction have been made. At low voltages the correction is entirely due to 1/f noise, while at high voltages, the correction is largely due to heating. In the mid-voltage range, both corrections are small. The solid line through the solid circles is the prediction of Eq. (2.13) using the measured values of R, I_o, I, V, and T. The upper dashed line is the predicted noise in the absence of zero point fluctuations, that is

$$\frac{S_V'(0)}{R_D^2} = \frac{4k_BT}{R} + \frac{4eV}{R}\left(\frac{I_o}{I}\right)^2 \frac{1}{\exp(2eV/k_BT) - 1} \tag{3.2}$$

The triangles in Fig. 3.4 represent the measured mixed-down noise, which was computed by subtracting $4k_BT/R$ from the solid circles. The solid line through the triangles is the mixed-down noise predicted by Eq. (2.13), $(2eV/R)(I_o/I)^2\coth(eV/k_BT)$, while the lower dashed line is the mixed-down noise predicted by Eq. (3.2) in the absence of zero point fluctuations, $(4eV/R)(I_o/I)^2\,[\exp(2eV/k_BT) - 1]^{-1}$. The small discrepancies between the data and Eq. (2.13) at very low voltages are possibly due to our neglect of noise rounding in the theory. It is evident from Fig. 3.4 that both the total measured noise across the junction and the measured mixed-down noise are in excellent agree-

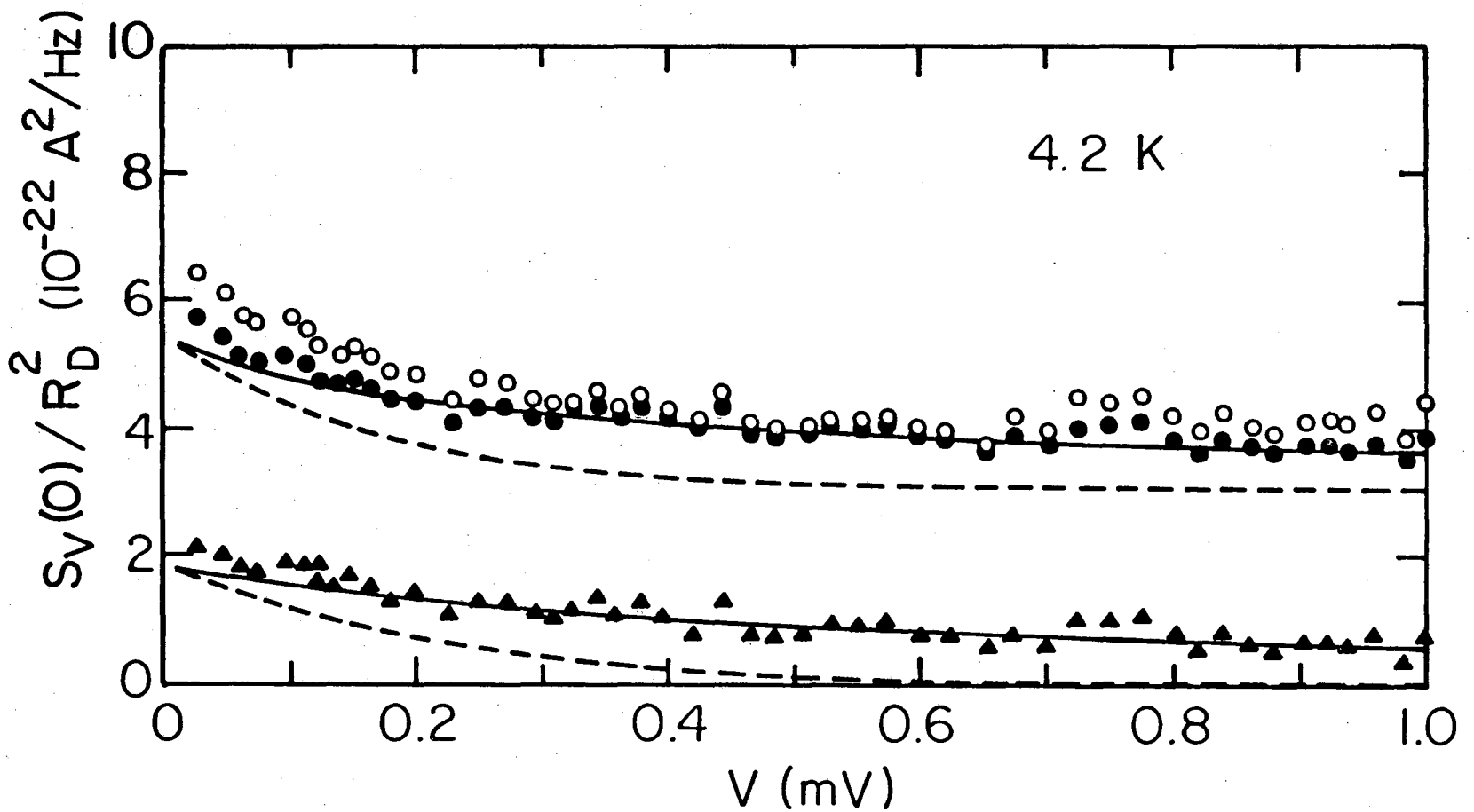

XBL817-6073

Fig. 3.4(a) $S_V(0)/R_D^2$ vs. V for junction 2 at 4.2K. The open circles show the total measured noise across the junction; solid circles below show the noise remaining after correction for 1/f noise and heating. Upper solid and dash lines are predictions of Eq. (2.13) and (3.2). Solid triangles are measured mixed-down noise, lower solid and dash lines are mixed-down noise predicted by Eqs. (2.13) and (3.2).

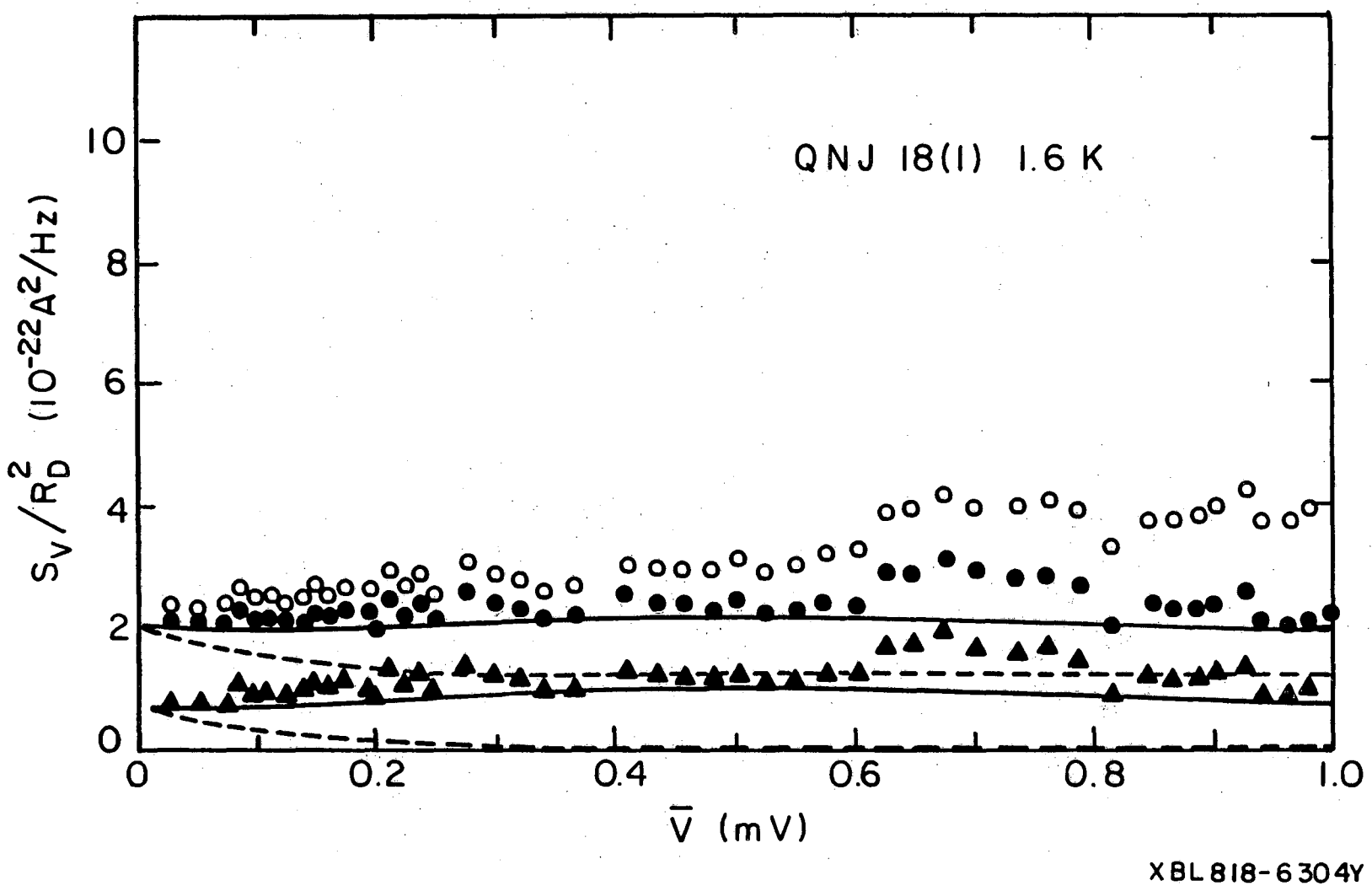

Fig. 3.4(b) $S_V(0)/R_D^2$ vs. V for junction 2 at 1.6K. Notation is as for Fig. 3.4(a).

ment with the theory that includes a contribution from the mixed-down zero point fluctuations, and are substantially higher than the predictions of a theory that does not include this contribution.

In Fig. 3.5 we show the temperature dependence of the noise for twelve bias voltages ranging from 50 μV to 550 μV. The notation is the same as that in Fig. 3.4. The temperature $T = 2eV/k_B$ is indicated for the six lowest voltages; mixed-down noise at temperatures well above this temperature is in the classical limit $eV \ll k_BT$, while that at temperatures well below this temperature is in the quantum limit $eV \gg k_BT$. The mixed-down noise at the six highest voltages is in the quantum limit at all temperatures measured. For all twelve voltages, the total junction noise is in good agreement with the predictions of Eq. (2.13), and substantially greater than the predictions of Eq. (3.2). The data at 300 μV, however, lie somewhat above the prediction. This discrepancy arises from the structure at 300 μV (see Fig. 3.3) that increases the magnitude of the mixed-down noise above the value predicted by Eq. (2.13) (this topic will be discussed in detail in Sec. III.2.D). The mixed-down noise at 350 μV and above is independent of temperature, and in excellent agreement with the value of Eq. (3.14), $S_v(0)/R_D^2 = (2eV/R)(I_o/I)^2$. (As the temperature was lowered, I_o increased slightly, giving rise to the slight increase in the mixed-down noise that is evident in both the data and the theoretical prediction.) As the voltage is lowered the mixed-down noise becomes increasingly temperature dependent, and remains in good agreement with the predictions of Eq. (2.13). At 50 μV, the mixed-down noise is in the classical limit for the whole temperature range, and proportional to T, as expected. This tempera-

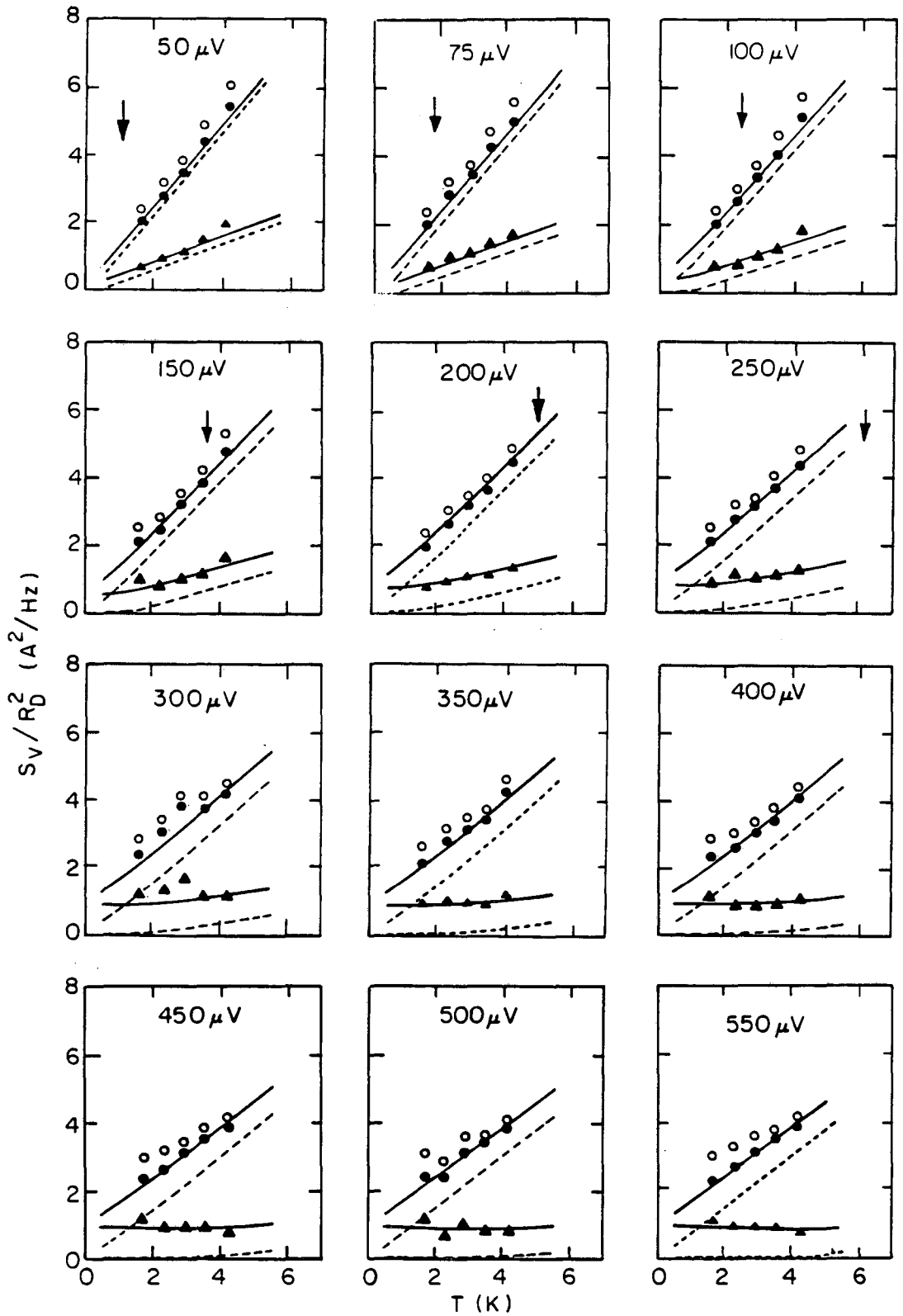

XBL819-6560

Fig. 3.5 $S_V(0)/R_D^2$ vs. T for junction 2 at 12 bias voltages. Notation is as for Fig. 3.4(a). Arrows indicate $2eV = k_BT$.

ture dependence demonstrates that the contribution of any extraneous noise was negligible.

We can extract from our data the measured spectral density of the current noise $S_I(\nu)$ generated by the shunt resistance R at the Josephson frequency $\nu = 2eV/h$. We divide each value of the mixed-down noise by the mixing coefficient $(I_o/I)^2/2$, a procedure that converts the mixed-down noise in Eq. (2.13) into Eq. (2.3). The results are plotted in Fig. 3.6 for 4.2K (solid circles) and 1.6K (open circles). The solid lines are the corresponding predictions of Eq. (2.3) using measured values of $\nu = 2eV/h$, R, and T. The slight increase of the data above the theory at the highest voltages may reflect the presence of a resonance on the I-V characteristic. The agreement between the data and the predictions is rather good, bearing in mind that, once again, no fitting parameters are used. By contrast, the dashed lines represent the theoretical prediction in the absence of the zero point term, $(4h\nu/R)\,[\exp(h\nu/k_BT) - 1]^{-1}$, and fall far below the data at the higher frequencies. The existence of zero point fluctuations in the measured spectral density of the current noise is rather convincingly demonstrated.

C. Junction 3

An alternative means of varying the mixed-down noise between the quantum and thermal limits is to change I_o at fixed temperature. The critical current was lowered by trapping flux in the junction. The 1/f noise in junction 3 at 183 kHz was insignificant (<2%), but the heating correction at the higher voltages was substantial, so that it was necessary to correct the mixed-down noise in addition to the noise

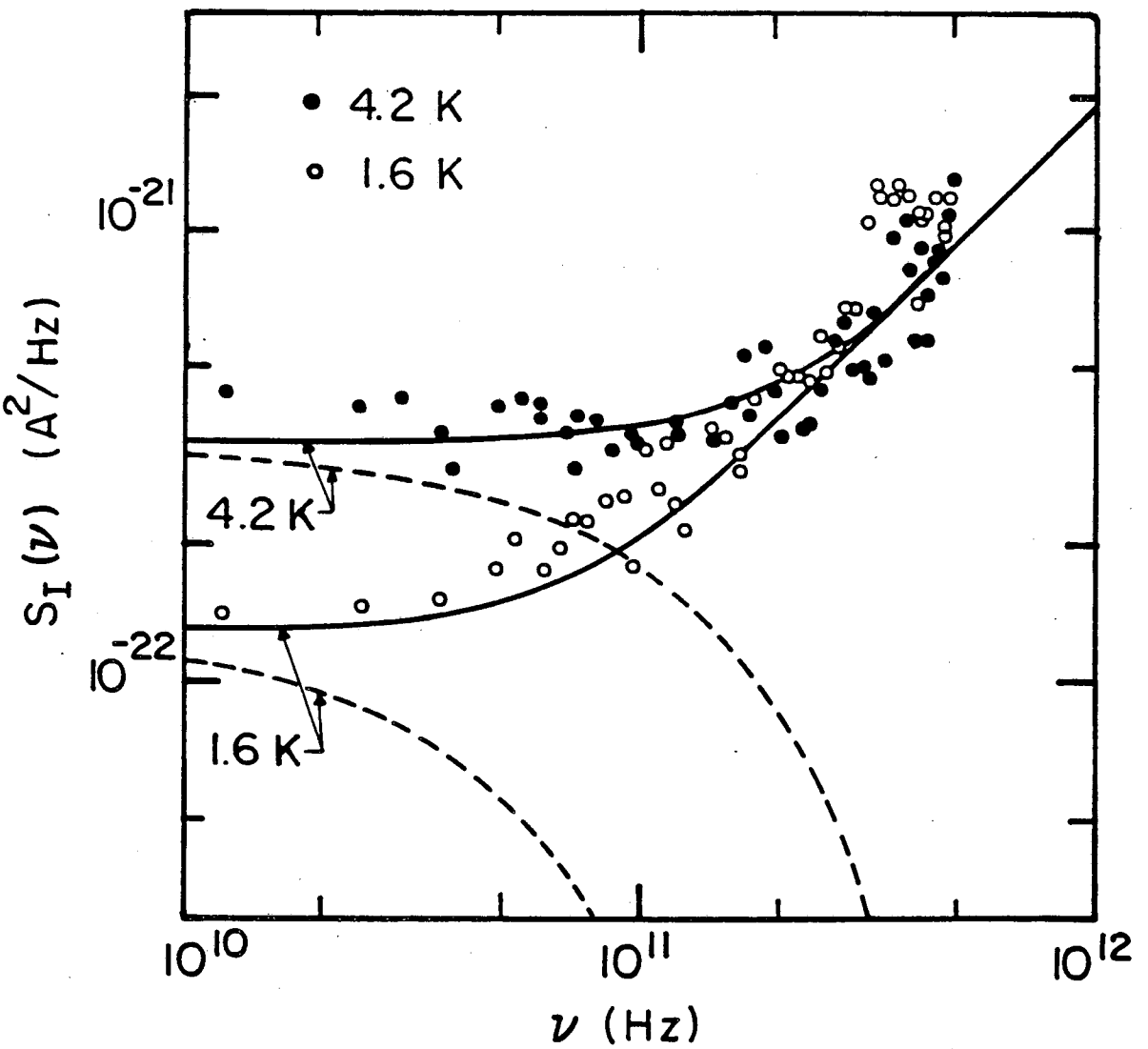

XBL 817-6072

Fig. 3.6 Measured spectral density of current noise in shunt resistor of junction 2 at 4.2K (solid circles) and 1.6K (open circles). Solid lines are prediction of Eq. (2.3), while dashed lines are $(4h\nu/R)$ $[\exp(h\nu/k_BT - 1]^{-1}$.

generated at the measurement frequency. In Fig. 3.7 we plot $S_v(0)/R_D^2$ vs. V at 4.2K for four values of I_o corresponding to values of κ ranging from 0.65 to 0.07. At the highest two values of I_o, the presence of a resonance near 200 μV increased the magnitude of the measured noise somewhat above the prediction of Eq. (2.13). Apart from this discrepancy, the measured total noise and the measured mixed-down noise are in very good agreement with the predictions. For $\kappa \approx 0.65$, the data lie convincingly above the theory that does not include the mixed-down zero-point fluctuations, while for $\kappa = 0.07$ the contribution of the zero-point term is less than our experimental error. Once again, the correct observed dependence of the noise on I_o demonstrates the absence of any significant extraneous noise.

D. Junction 4

As noted earlier, some junctions contain resonances that can affect the magnitude of the noise mixed down to the measurement frequency. Junction 4 exhibited strong resonant structure, and we have investigated its origin and its effect on the noise in some detail. Figure 3.8 shows the I-V and (dV/dI) - V characteristics at 1.1K for four values of critical current; the three lowest values were obtained by trapping flux in the junction. The structure arises from the resonant circuit formed by the shunt inductance, L_s, and junction capacitance, C; the equivalent circuit is shown in the inset in Fig. 3.9. The resonant circuit pulls the Josephson frequency slightly so that it becomes more closely a subharmonic of the resonant frequency. Hence, as the current bias is increased, the dynamic resistance will be alternately increased and decreased as the Josephson frequency passes through

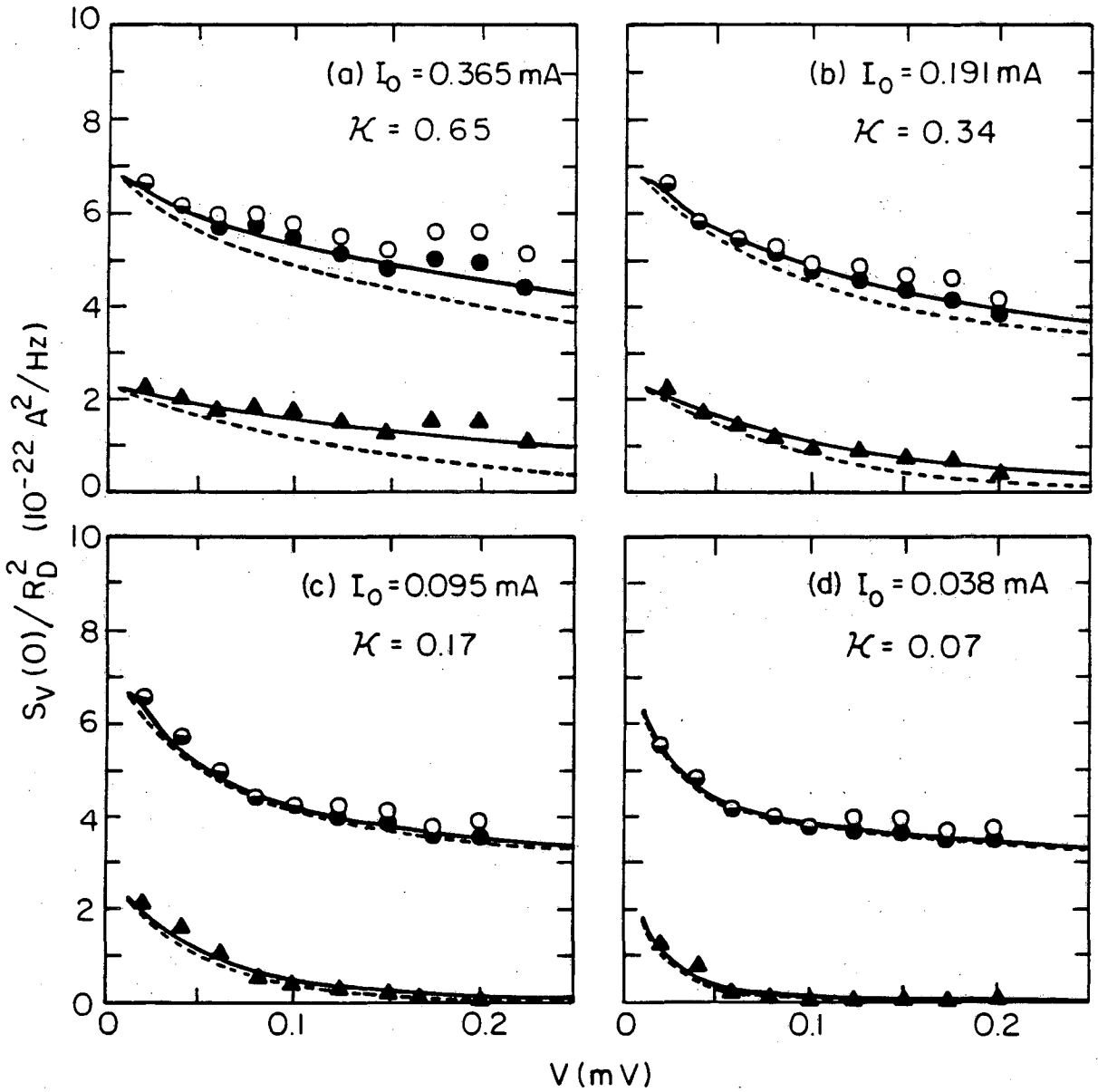

Fig. 3.7 $S_V(0)$ vs. V for junction 3 at 4.2K for 4 values of I_0. Notation is as for Fig. 3.4(a).

each subharmonic frequency of the LCR resonance. The 1/n dependence of the dynamic resistance is shown clearly in Figs. 3.8 and 3.9 (n is an integer).

The equations of motion are

$$I = I_o \sin\delta + C\dot{V} + I_s \ , \tag{3.3}$$

and

$$V = I_s R + \dot{I}_s L_s + V_N \ , \tag{3.4}$$

where I_s is the current flowing through the shunt, and V_N is the equilibrium noise voltage generated by R with spectral density $2h\nu\ R\coth(h\nu/2k_B/T)$. We have computed the I-V characteristics and the spectral density of the voltage noise across the junction, using the procedure outlined in Appendix A. To obtain these curves, it was necessary to fit the values of L_s and C. From our simulations, we conclude that the I-V characteristic will show substantial resonant structure when $\beta_L = 2\pi L_s I_o/\Phi_o \gtrsim 0.5$ and the approximate Q of the LCR circuit $(\beta_L/\beta_c)^{1/2} >> 1$. The observed rapid decrease in the magnitude of the resonant structure as I_o is lowered is demonstrated in Fig. 3.8.

Figure 3.9 shows I and R_D vs. V for junction 4 at 1.4K, the temperature at which the noise measurements were made. The computed dynamic resistance is also shown, using L_s = 0.23 pH and C = 0.81 pF; these values are consistent with values expected from the dimensions of the sample. The agreement between the measured and computed values is quite good, although the measured structure at the higher voltages is considerably more smeared than predicted, possibly because of noise

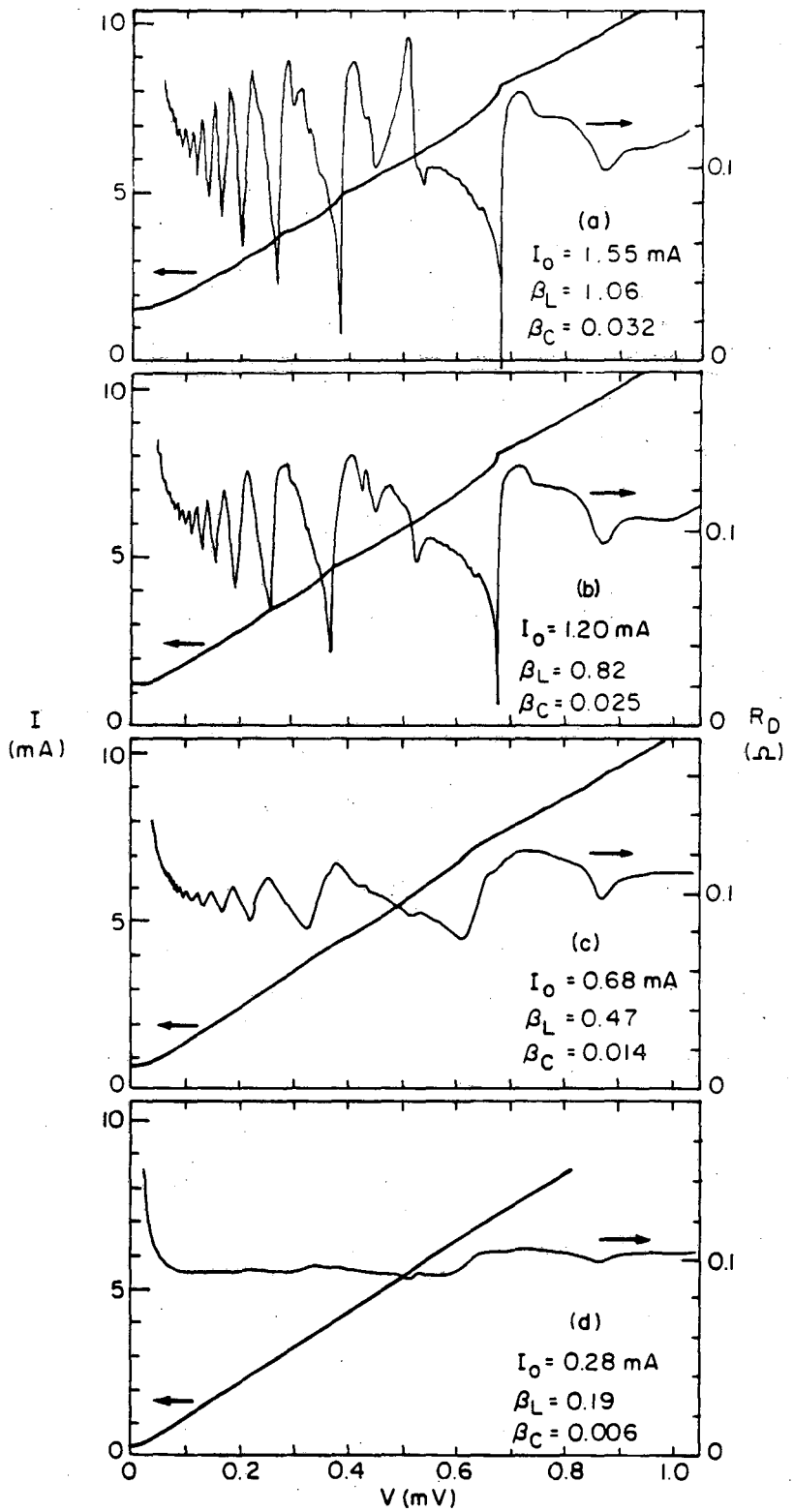

Fig. 3.8 I-V and dV/dI-V curves for junction 4 at 1.1K for four values of I_o.

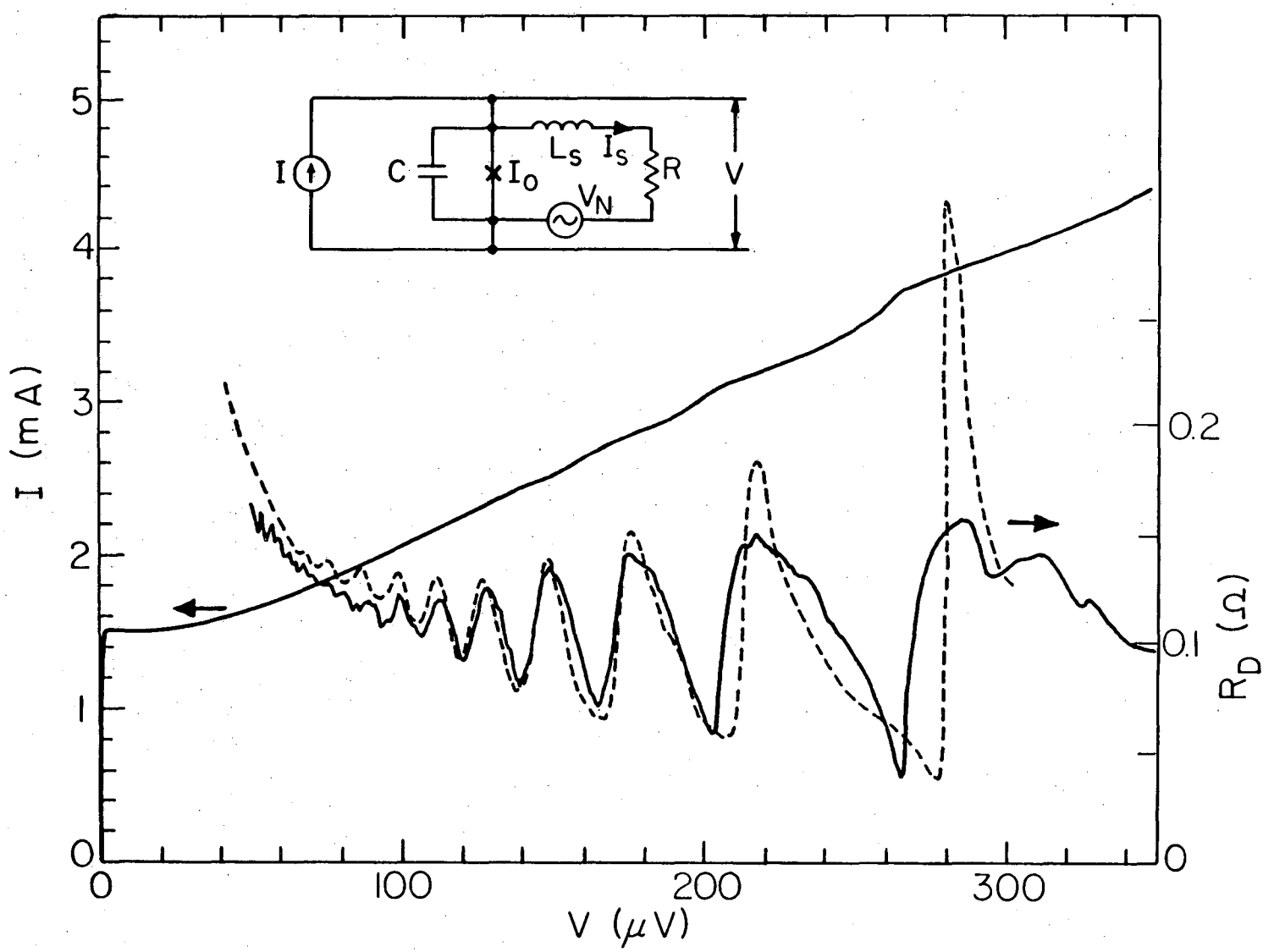

XBL 811-5036A

Fig. 3.9 I and R_D vs. V for junction 4 at 1.4K with I_0 = 1.53 mA, R = 0.092Ω, κ = 1.17, β_L = 1.05, and β_c = 0.032. Dashed line is computed R_D. Inset is equivalent circuit of junction.

rounding. Furthermore, the measurements lie slightly below the computed values at lower voltages, even though noise rounding is negligible in this region. This discrepancy occurs because the measured shunt resistance at low voltages dropped somewhat below the high voltage value, a fact that could not readily be included in the computer simulation.

This junction was investigated at an early stage of our work, and we measured the noise mostly at one frequency only, 98.6 kHz, with a few measurements at 31.6 kHz. We used the following procedure to subtract the 1/f noise in the range of voltage where the oscillations occured. First, if the 1/f noise arises from fluctuations in the critical current (Clarke and Hawkins, 76) the spectral density of the voltage noise should be proportional to $(\partial V/\partial I_o)^2$. At voltages where the RSJ result, Eq. (2.2), is valid we find

$$\left(\frac{\partial V}{\partial I_o}\right)^2 = R^2\left(\frac{I_o R}{V}\right)^2 \quad . \tag{3.5}$$

Hence, the voltage noise arising from 1/f fluctuations will be

$$S_V^{1/f}(\nu) = R^2(I_o R/V)^2 S_{I_o}^{1/f}(\nu) \quad , \tag{3.6}$$

where $S_{I_o}^{1/f}(\nu)$ is the spectral density of the 1/f fluctuations in the critical current at the measurement frequency. Second, the mixed-down noise in Eq. (2.1) for voltages well below $k_B T/e$ can be written as $(2k_B TR)(I_o R/V)^2$. Thus, at low voltages where the deviations from the RSJ model are negligible and for fixed values of I_o, R and T, the spectral densities of both the mixed-down noise and 1/f noise (and their

sum) should be proportional to $1/V^2$. Figure 3.10 shows the spectral densities of the voltage noise across the junction for $V < 100\ \mu V$ at 98.6 kHz, and for two voltages at 31.6 kHz, with the direct term $(4k_BT/R)R_D^2$ subtracted out. At 98.6 kHz the plotted quantity scales with $1/V^2$, suggesting that the 1/f noise scales as $(\partial V/\partial I_o)^2$. We then assume that the spectral density of the excess noise scales as 1/f, and from data at the two voltages where measurements were made at two frequencies, calculate the spectral density of the 1/f noise in the critical current: $S_{I_o}^{1/f}(98.6\ \text{kHz}) = 5.5 \times 10^{-22}\ A^2Hz^{-1}$. By subtracting the 1/f voltage noise computed using Eq. (3.6) from the data at 98.6 kHz, we obtain the mixed-down noise shown in Fig. 3.10. The mixed-down noise is in excellent agreement with the predicted value. Thus, this procedure provides strong evidence that the spectral density of the excess noise at low voltages scales closely as 1/f (as is the case for all junctions on which we have measurements at three frequencies). We then calculated the 1/f voltage noise at the higher voltages (> 100 μV) from measurements at 98.6 kHz, using the value of $S_{I_o}^{1/f}$ quoted above, together wih measured values of $\partial V/\partial I_o$. We also measured the noise at 31.6 kHz at several voltages between 100 and 200 μV, and obtained values that were consistent with those obtained by the above procedure. Since the overall 1/f correction was small, typically 15% or less of the total junction noise at 200 μV, we believe that the error introduced by the correction is at most ±5% of the mixed-down noise.

As a further complication, we did not measure the heating correction on this junction, but rather on one fabricated simultaneously.

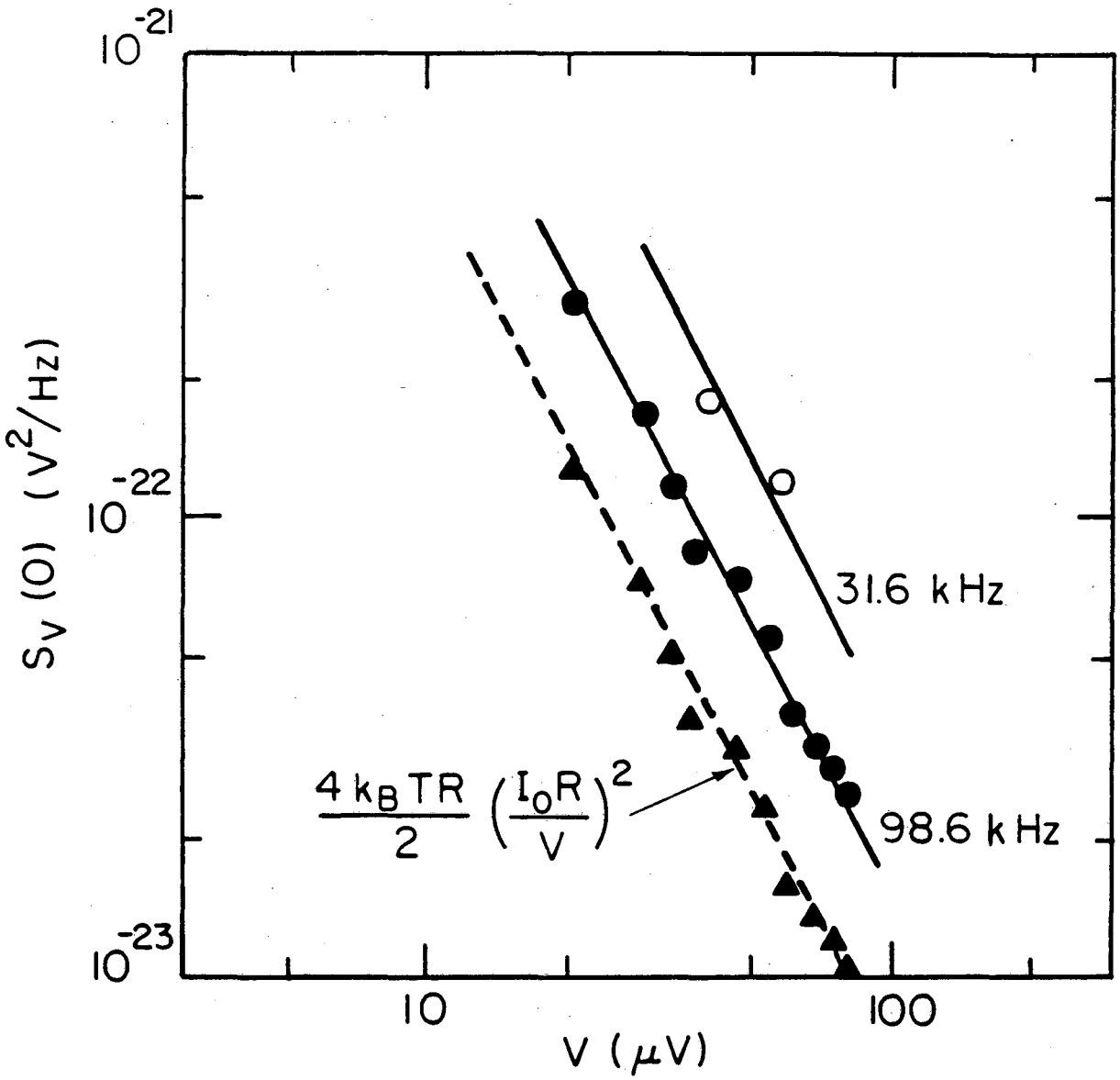

XBL 818-6314

Fig. 3.10 Spectral density of total voltage noise across junction 4 at two frequencies in the region $V < k_BT/e$ with $(4k_BTR_D^2/R)$ subtracted out (open and solid circles). Solid lines have slope - 2. Triangles are measured mixed-down noise assuming excess low frequency noise is proportional to 1/f; dashed line is prediction of Eq. (2.1).

As a result the heating correction had a higher uncertainty, which we estimate to be $\pm 6\%$ of the total spectral density, than for the other junctions.

Figure 3.11(a) shows the spectral density of the measured voltage noise at 1.4K, together with the measured mixed-down noise computed by subtracting $4k_B TR_D^2/R$, with the 1/f noise subtracted. The solid line shows the result of the computer simulation, with the zero point term included and with the values of L_s and C obtained by fitting the model to the I-V characteristics in Fig. 3.10. The data tend to lie somewhat above the computed curve at voltages above 100 V. In Fig. 3.11(b) we have applied a heating correction by subtracting $4k_B \Delta TR_D^2/R$ from the solid circles in 3.11(a). The agreement between the measured and computed values is now rather good, indicating that our model is a good approximation.

Our computer simulation yields the magnitudes of the contributions of the noise generated at multiples of the Josephson frequency, as shown in Fig. 3.12. We define a mixing impedance, Z_k, (Likharev and Semenov, 72) via the relation

$$S_v(0) = \sum_{k=0}^{\infty} S_v^{(k)}(0) = \sum_{k=0}^{\infty} |Z_k|^2 S_I(k\nu_J) , \qquad (3.7)$$

where k = 0, 1, 2 ..., and $S_v^{(k)}(0)$ is the spectral density of the mixed-down voltage noise due to noise near frequency $k\nu_J$. We note that $|Z_o|^2 = R_D^2$. For $\beta_c = 0.031$ and $\beta_L = 0.05$, A_k is essentially zero for $k \geqslant 2$, and the deviations from the RSJ model are negligible. On the other hand, for $\beta_L = 0.4$ and 1.05, there are very substantial

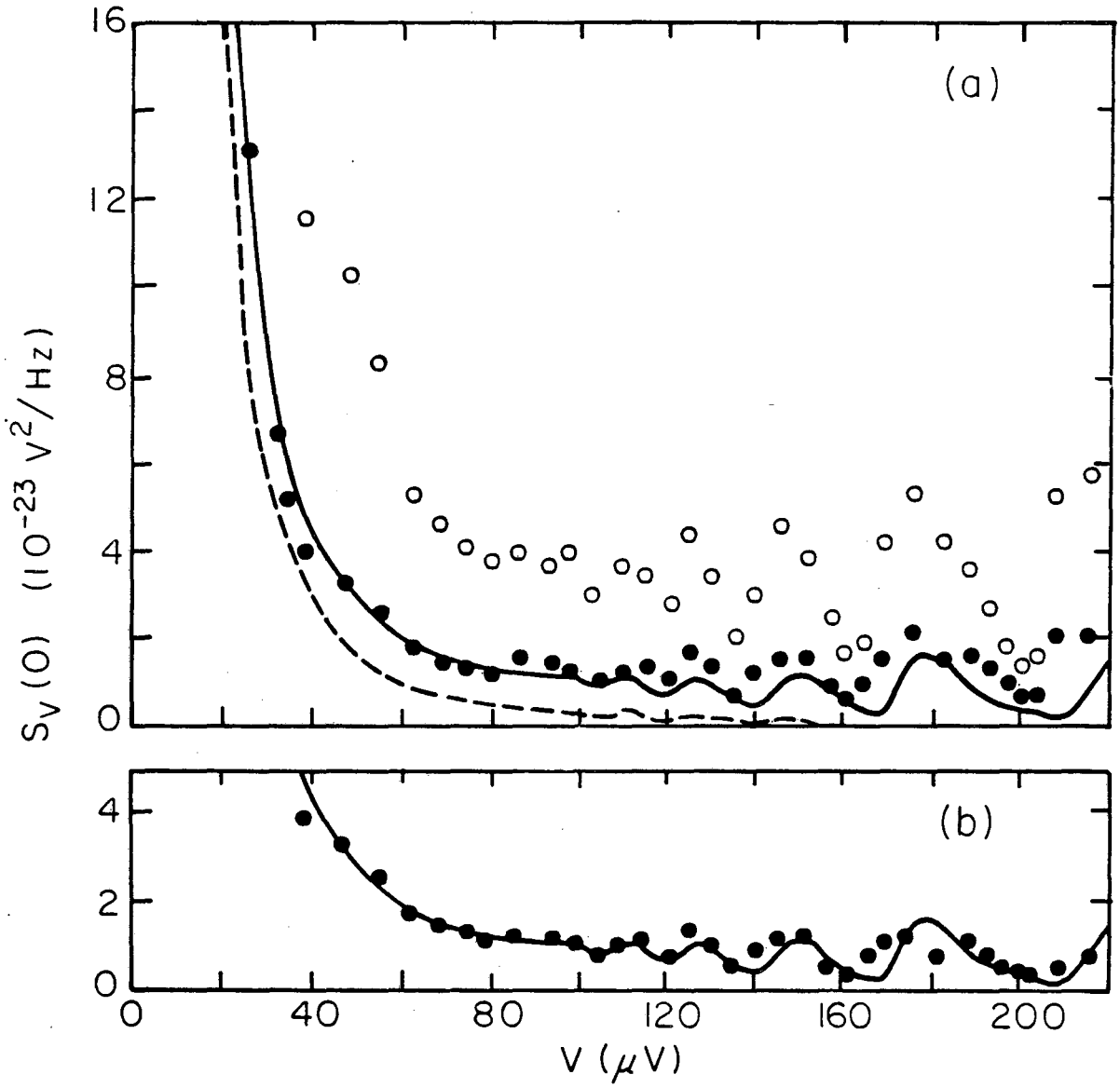

XBL 811-5035

Fig. 3.11 (a) Open circles are measured voltage noise across junction 4 at 1.4K, solid circles are mixed-down noise with 1/f noise subtracted. Solid and dashed lines are predictions of computer simulation with and without zero-point term. (b) Solid circles are data after heating correction has been made, solid line is identical to that in (a).

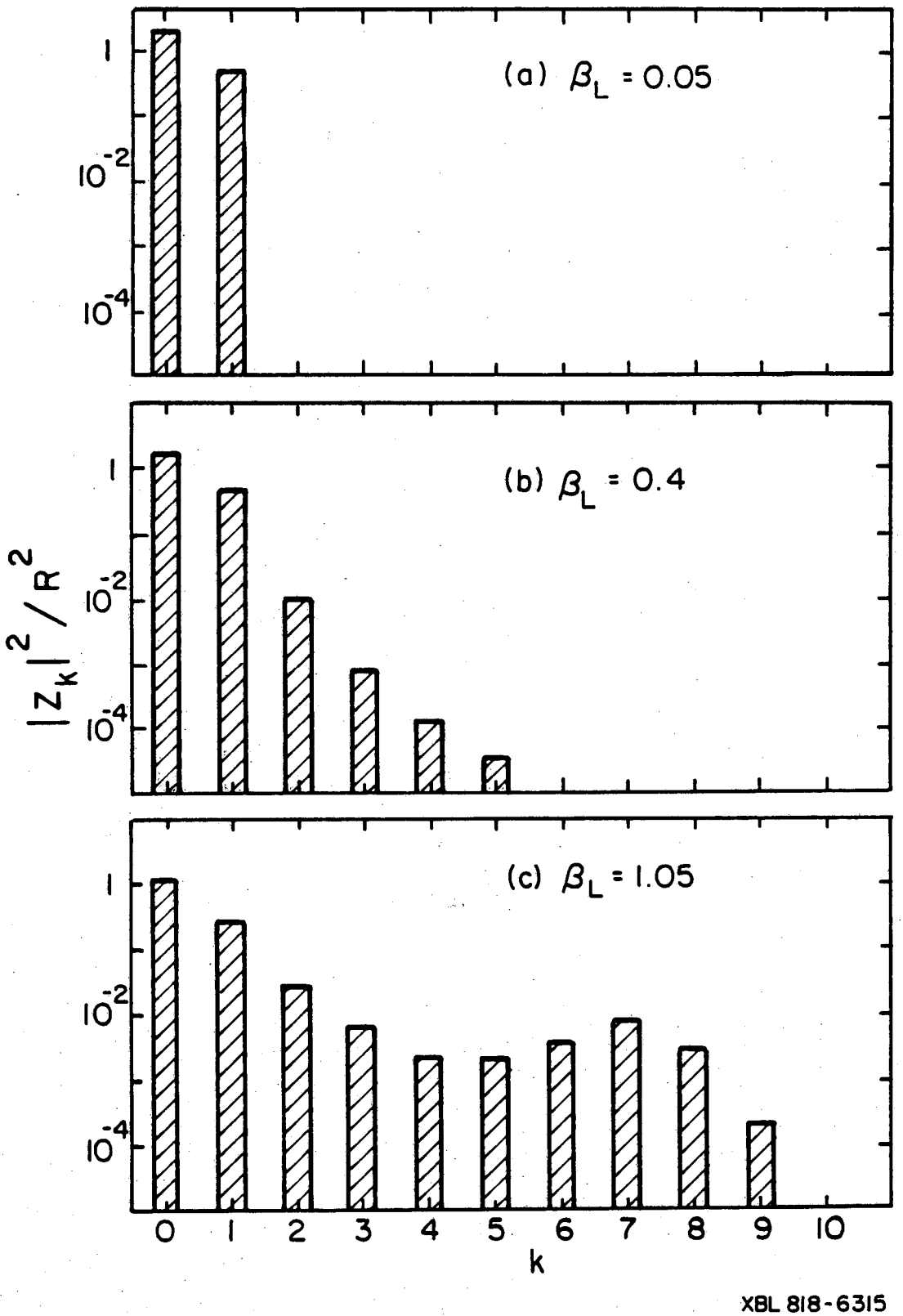

Fig. 3.12 $|Z_k|^2/R^2$ for a junction with β_c = 0.031 for 3 values of β_L and a bias current I/I_o = 1.42.

contributions to the noise from harmonics out to the 5th and 9th, respectively, and the noise is considerably enhanced over the value predicted by Eq. (2.13). These results explain quantitatively the additional noise associated with the resonant structure, and, qualitatively, the additional noise observed on junctions 2 and 3 in the vicinity of structure on the I-V characteristic. In fact, the capacitance and inductance of these two junctions were estimated from computer fits to this structure.

Although the data obtained from junction 4 are considerably harder to interpret than those from the other junctions, the role of zero point fluctuations is even more important because of the large number of harmonics that contribute to the mixed-down noise. The noise generated at frequencies near the higher harmonics can be in the quantum limit even for junctions with $\kappa < 1$.

3. Concluding Remarks

We emphasize that in comparing the data for junctions 1, 2, and 3 with theory we have used only measured parameters; there is no fitting of the data. Thus, junctions 2 and 3 provide the main evidence for the accuracy of Eq. (2.13). We believe the results obtained from these junctions are a convincing demonstration first, of the existence of a zero point term in the spectral density of the current noise of a resistor in thermal equilibrium (Fig. 3.6), and, second, that these fluctuations give rise to the limiting voltage noise in a current-biased resistively shunted Josephson junction in the quantum limit for $I > I_o$ (Figs. 3.4, 3.5 and 3.7). Furthermore, the good agreement between our results and Eq. (2.13) justifies our use of a Langevin

equation together with a zero-point driving term to predict quantum noise effects in a current-biased Josephson junction in the overdamped limit when it is in the free-running mode $I > I_o$. We were not able to examine the validity of the theory in the noise-rounded case $I < I_o$ since quantum effects are negligible in this regime in the He^4 temperature range for the parameters of our junctions.

The data from junction 4, which exhibited resonant structure, require a fitting of L_s and C to compare the experimental results with the theory. However, we note that the values of L_s and C that yield an excellent fit to the measured I and dV/dI vs. V characteristics, also produce a very good fit to the noise data (Fig. 3.11). These results show very dramatically the strong effects of additional non-linearities on the voltage noise due to the mixing-down of higher order harmonics. Because quantum effects increase rapidly as the order of the harmonic increases, the role of zero-point fluctuations is even more pronounced in junctions with resonant structure.

The fact that the zero-point fluctuations in the resistor can be observed at frequencies as high as 5×10^{11} Hz implies that a Josephson mixer using the ac Josephson effect as the local oscillator is an ideal quantum-limited device at these frequencies. When an external local oscillator is used, however, the additional non-linearity induced on the I-V characteristic causes noise near the higher harmonics of the Josephson frequency to be mixed down, thereby greatly increasing the noise of the mixer. This limitation of the Josephson mixer with an external local oscillator has been discussed extensively by other authors (Taur, 80; Claassen and Richards, 78).

Finally, in accord with other observations, (Giffard et al., 79; Claassen, et al., 74) we find no evidence for a contribution to the measured noise arising from the shot noise of pairs tunneling through the junction. For example, in Fig. 3.4, the spectral density of a term $4eI_o$ would be about 3.2×10^{-22} A^2Hz^{-1}, a value at least five times greater than the observed mixed-down noise at 1 mV. We emphasize, however, that this observation in no way invalidates the theory of Stephen, (1969) which is applicable to a quite different situation.

Table 3.1. Parameters of Junctions.[a,b]

Junction	1	2		3	4
Temperature (K)	4.2	4.2	1.6	4.2	1.4
I_o (mA)	0.32	0.51	0.60	0.36	1.53
R (Ω)	0.075	0.67Ω at 50μV		0.58Ω at 50μV	0.084Ω at 50μV
		0.70Ω at 100μV		0.62Ω at 100μV	0.092Ω at 100μV
		0.75Ω at 400μV		0.68Ω at 200μV	
				0.77Ω at 400μV	
β_c	0.003	0.38	0.45	0.21	0.032
β_L	0.20	0.31	0.37	0.22	1.05
κ	0.066	0.99	3.0	0.62	1.17
$S_{I_o}^{1/f}(A^2Hz^{-1})$	$<2 \times 10^{-22}$	6.0×10^{-23}	3.0×10^{-23}	$<3 \times 10^{-24}$	5.5×10^{-22}
(frequency)	(100kHz)	(183kHz)	(183kHz)	(183kHz)	(100kHz)
Heating (K/μW)	<1	0.25	1.6	7	1.6

[a]C = 0.5 pF for 1, 2, 3, 0.81 pF for 4; R taken at 100μV.

[b]L = 0.2 pH for 1, 2, 3, 0.23 pH for 4; taken at 100 μV.

IV. DC SQUID THEORY

Recent research on dc superconducting quantum interference devices (SQUID's) has been directed toward the fabrication of a device limited in sensitivity by intrinsic quantum mechanical noise processes. In this section we present a model calculation of the noise in the dc SQUID that involves the complete quantum expression for the equilibrium noise in the shunt resistance of each junction. At T = 0, where the sensitivity is limited by zero-point fluctuations in the shunt resistances, for an optimized SQUID we find an equivalent noise energy $\varepsilon/1\text{Hz} = S_\Phi/2L \approx \hbar$, where S_Φ is the spectral density of the equivalent flux noise, and L is the SQUID inductance. When the SQUID is coupled to an optimized series-resonant input circuit, we find total equivalent noise power referred to the input to be $h\nu$, where ν is the signal frequency. This noise power represents the uncertainty principle limit for any linear amplifier, and thus the system operates nearly as an ideal amplifier at T = 0. We show that by proper choice of parameters it should be possible to approach this ideal behavior with a SQUID operated at 1 K.

Tesche and Clarke (1977) calculated $\varepsilon/1\text{Hz}$ for a SQUID incorporating two resistively shunted Josephson junctions (RSJ) with zero capacitance assuming that the only source of noise was thermal noise in the resistive shunts. Their predictions have subsequently been found to be in reasonable accord with experimental measurements (Clarke, 80). In the absence of any rigorous calculation of the limiting voltage noise in a current-biased RSJ at T = 0, they speculated that the ultimate sensitivity should be limited by pair shot noise in the tunnel junc-

tions. Assuming a shot noise voltage spectral density $2eI_oR^2$ for a junction with critical current I_o and shunt resistance R, they found $\varepsilon/1\text{Hz} = h/2$ for an optimized SQUID. However, we now suggest that the noise in an overdamped RSJ at T = 0 is set by zero-point fluctuations in the shunt resistance rather than by an intrinsic shot noise in the junction itself (Gallop and Petley, 76). We now apply the zero-point fluctuation calculation, including the effects of junction capacitance, to the case of the SQUID.

1. The Model

We begin by considering the isolated symmetric SQUID. Each of the two junctions has a critical current I_o, capacitance C, and shunt resistance R. We introduce the dimensionless parameters $\beta_c \equiv 2\pi I_o R^2 C/\Phi_o$, $\beta \equiv 2LI_o/\Phi_0$, $\kappa \equiv eI_0R/k_BT$ and $\Gamma \equiv 2\pi k_B T/I_0\Phi_0$. The phase differences across junctions 1 and 2, δ_1 and δ_2, and the voltage V(t) across the SQUID are related to the circulating current J(t) and applied flux Φ by the equations

$$J/I_0 = (\delta_1 - \delta_2 - 2\pi\Phi/\Phi_o)\pi\beta \quad , \tag{4.1}$$

$$V = (\dot{\delta}_1 + \dot{\delta}_2)\Phi_o/4\pi, \tag{4.2}$$

$$\beta_c \frac{\ddot{\delta}1}{I_o}\left(\frac{\Phi_o}{2\pi R}\right)^2 + \dot{\delta}1\left(\frac{\Phi_o}{2\pi R}\right) = \frac{I}{2} - J - I_o \sin\delta_1 + I_{N1} \ , \tag{4.3}$$

$$\beta_c \frac{\ddot{\delta}2}{I_o}\left(\frac{\Phi_o}{2\pi R}\right)^2 + \dot{\delta}2\left(\frac{\Phi_o}{2\pi R}\right) = \frac{I}{2} + J - I_o \sin\delta_1 + I_{N2} \ , \tag{4.4}$$

Here, I_{N1} and I_{N2} are the equilibrium noise currents generated in the shunt resistors, each with a spectral density $(2h\nu/R)\coth(h\nu/2k_BT)$,

which includes zero-point fluctuations. To find the limiting performance, we first solve Eqs. (4.1)-(4.4) numerically to obtain ε/1Hz and T_N for a SQUID at T = 0 with $\kappa\Gamma = 0.02$ ($R \approx 40\Omega$) and $\beta = 1$; at T = 0, the spectral density of the current noise in each shunt resistor reduces $2h\nu/R$. The computer techniques used were similar to those described for the single junction calculations.

2. Results

Figure 4.1(a)-(f) shows the time-averaged voltage V, the transfer function $\partial V/\partial\Phi$, the noise spectral densities S_V, S_J, S_{VJ}, and ε/1Hz vs Φ for three values of β_c where S_V and S_J are the spectral densities of the voltage noise across and the current noise around the SQUID; S_{VJ} is the cross-spectral density of these two noises (Tesche and Clarke, 79), and $\varepsilon/1\text{Hz} = S_\Phi/2L$, where $S_\Phi = S_v/(\partial V/\partial\Phi)^2$. The current I, which has the same value of $1.63I_o$ for all the curves, has been chosen so that the maximum in $\partial V/\partial\Phi$ always occurs near $\Phi = \Phi_o/4$. In a separate investigation, we have found that this procedure produces the optimum performance. The peaks in the noise spectral densities occur at slightly different values of applied flux than the peak in $\partial V/\partial\Phi$. As β_c is increased from 0.25 to 1, the maximum values of $\partial V/\partial\Phi$ and S_V, S_J, and S_{VJ} all increase markedly. However, the minimum values of ε/1Hz are remarkably close to each other, reflecting the fact that $(\partial V/\partial\Phi)^2$ and S_V increase almost proportionately as β_c is changed with R held constant. The minima in ε/1 Hz, about $\hbar$ in all three cases, are much broader with respect to the applied flux than the peaks in $\partial V/\partial\Phi$ and the noise spectral densities.

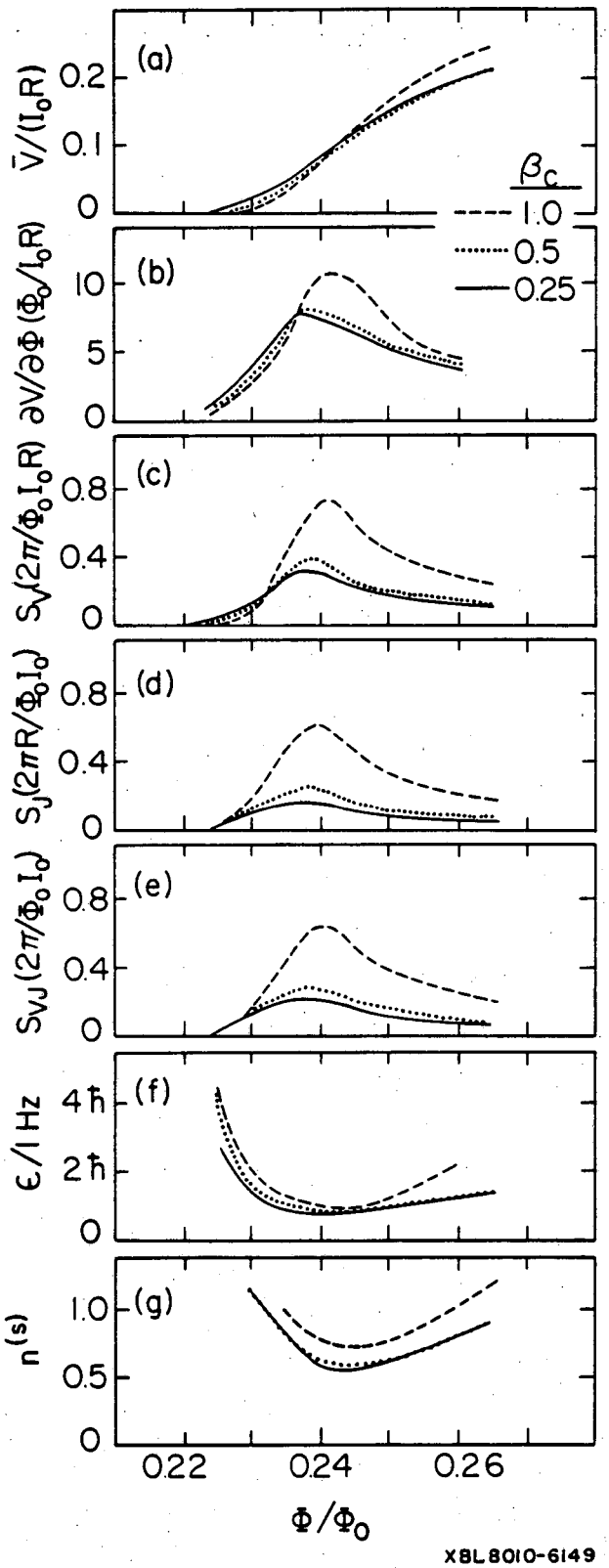

Fig. 4.1 Computed values of V, $\partial V/\partial\Phi$, S_V, S_J, S_{VJ}, $S_\Phi/2L$, and $n^{(s)}$ vs. Φ/Φ_o for a dc SQUID at T = 0 with $\kappa\Gamma = 0.02$, $\beta = 1$, a bias current of $1.63I_o$, and for $\beta_c = 0.25$, 0.5 and 1. Computed values are accurate to $\pm$ 15%.

We have not included in these calculations the possibility of Macroscopic Quantum Tunnelling which could permit the SQUID to tunnel between wells of metastable equilibrium that exist when $|I| < I_c$ (Tesche, 1981). One might expect this effect to be important since the SQUID performance peaks approximately at $I \sim I_c$ (I_c is the critical current of the SQUID for a given applied flux. $I_c \leqslant 2I_o$). However since MQT is predicted to decrease rapidly as the damping increases, we do not expect it to make a significant contribution in the highly damped limit considered here. See Section II.2 for more details.

3. Ultimate Performance at T = 0

The quantity ε/1Hz is a convenient parameter for comparing the performance of isolated SQUID's, but does not completely specify the sensitivity of the device. In practice, the SQUID must be coupled to an input circuit, and one must take into account not only S_V, but also S_J and S_{VJ}. The current noise of the SQUID couples back to the input coil, producing a real voltage noise at the input terminals, while the voltage noise of the SQUID can be regarded as an effective noise referred to the input. In Clarke, Tesche, and Giffard (CTG) (1979), it was shown that the tuned input circuit shown in Fig. 4.2 has a higher sensitivity than an untuned circuit. For a given source resistance R_i, the values of L_i and C_i have been optimized for a signal frequency $\nu \ll 2eV/h$. From Eqs. (15) and (16) of CTG, it is straightforward to show that the SQUID introduces (in a weak coupling limit, $\alpha^2 \equiv M^2/(LL_i) \ll 1$,) a total effective voltage noise referred to the input terminals of the voltmeter with a spectral density. (See the appendix for the corrections in the tightly coupled case $\alpha^2 \sim 1$).

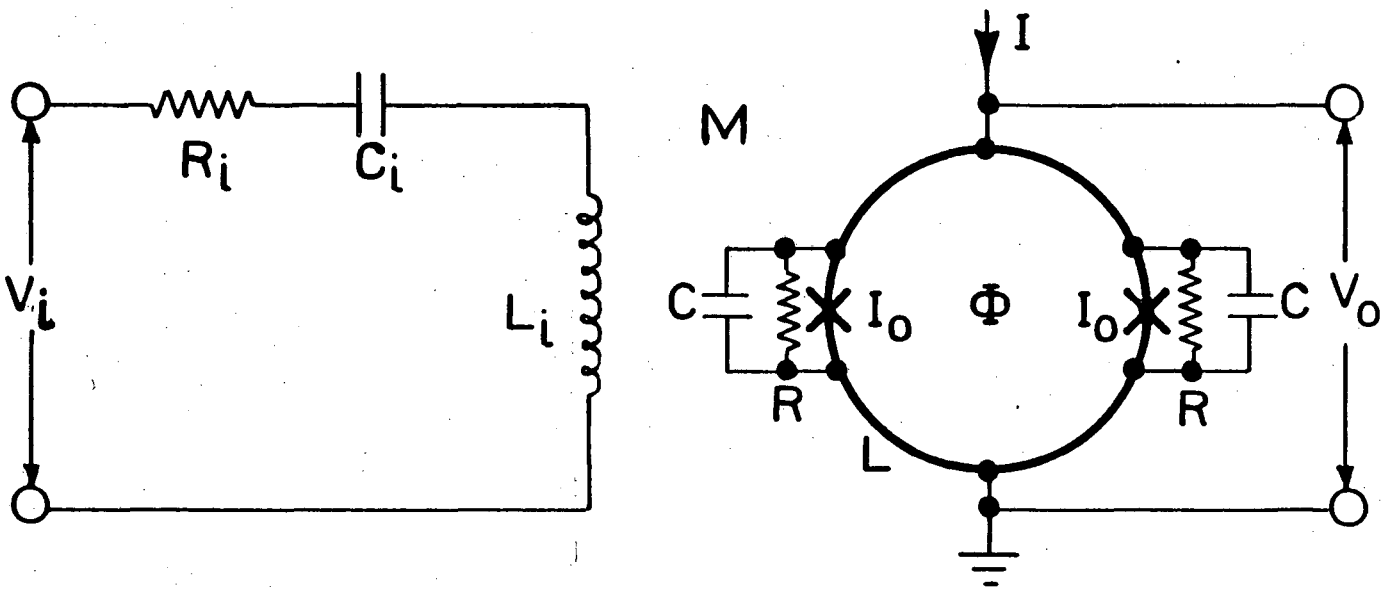

XBL 8010-6148

Fig. 4.2 Schematic of dc SQUID coupled to tuned input circuit; V_i and V_o are the input and output voltages. $M^2 = \alpha^2 L L_i$.

$$S_V^{(s)}(\nu) = 4\pi\nu R_i \left(\frac{\partial V}{\partial \Phi}\right)^{-1} (S_V S_J - S_{VJ}^2)^{1/2} \tag{4.5}$$

We define the quantity $n^{(s)}h\nu = S_V^{(s)}(\nu)/4R_i$ as the effective mean photon power per hertz in the input circuit due to intrinsic SQUID noise. Thus

$$n^{(s)} = \pi(S_V S_J - S_{VJ}^2)^{1/2} \left(\frac{h\partial V}{\partial \Phi}\right)^{-1} \tag{4.6}$$

In Fig. 1(g), we plot $n^{(s)}$ vs Φ. We see that for $\beta_c = 0.25$ and 0.5, $n^{(s)}$ has the minimum value of ~1/2, whereas for $\beta_c = 1$, the minimum has a somewhat higher value. Thus for $\beta_c = 0.25$ and 0.5, an optimized tuned voltmeter at T = 0 has a mean input noise due to the intrinsic SQUID noise of 1/2 photon at the measurement frequency. At a signal frequency ν, we add the SQUID noise in the input circuit, $h\nu/2$, to the zero-point fluctuations of the input resistor, $h\nu/2$; their sum, $h\nu$, approximately equals the minimum value for any linear phase-preserving amplifier. (Louisell, et al, 71; Gordon, et al, 63; Caves, preprint).

The intrinsic noise can be expressed alternatively as a noise temperature. We equate the sum, $h\nu$, to the thermal noise power per Hz available from the resistor at an effective temperature T_N, namely $h\nu/[\exp(h\nu/k_B T_N) - 1]$. We thus obtain

$$T_N \approx h\nu/k_B \ln 2, \tag{4.7}$$

the optimum value for any linear amplifier (Louisell et al; 61).

4. Results for $T \neq 0$

We now consider briefly the experimentally realistic case $T \neq 0$. In Table 4.1 we list values of $\partial V/\partial\Phi$, $\varepsilon/1\text{Hz}$, and $n^{(s)}$ for a SQUID with an inductance of 1 pH and a capacitance of 0.5 pF per junction (corresponding to a junction area of about $10\mu m^2$), for specified values of T, β, I_o, β_c and R. We also list $\kappa V/I_0R$, the parameter characterizing the relative importance of the quantum and thermal noise sources, and $\Delta\Phi/\Phi_o$, a measure of the applied flux over which the quoted sensitivity can be obtained. For the computations at 4.2 K we used the classical limit $4\ k_BT/R$ for the spectral density of the current noise in each shunt, whereas at the lower temperatures we used the full expression $(2h\nu/R)\coth(h\nu/2k_BT)$. At 4.2 K, the values of $\varepsilon/1\text{Hz}$ range from about $3\hbar$ to $11\hbar$, while the values of $n^{(s)}$ range from about 4.5 to 9. The lowest values of $n^{(s)}$ due to the effects of current noise. We have also computed the sensitivity at T = 0.9 and 0.45 K for the values $\beta = \beta_c = 1$, and find $n^{(s)} = 2.0$ and 1.5, respectively. It is interesting to note that the SQUID approaches the quantum limit when $\kappa V/I_oR \approx 1$, as we would expect from our analysis of the single junction. As one goes to lower temperatures, the range of applied flux, $\Delta\Phi/\Phi_o$, over which the best sensitivity is obtained narrows from 0.005 at 4.2 K to 0.001 at the lower temperatures.

5. Concluding Remarks

In conclusion, we have shown that at T = 0 a dc SQUID coupled to a tuned input circuit has a noise temperature of $h\nu/k_B\ln 2$, corresponding to an intrinsic photon power per Hz of $h\nu$, when the parameters are properly optimized. At a temperature of 1K, one should be able to

Table 4.1. Parameters for SQUID with L = 1 pH and C = 0.5 pF. Computed values accurate ± 15%.

T (K)	β	I_o (mA)	β_c	R (Ω)	$\kappa V/I_oR$	$\partial V/\partial\Phi$ (mV/Φ_o)	ε/1Hz ($\hbar$)	$n^{(s)}$	$\Delta\Phi/\Phi_o$
4.2	0.5	0.5	1.0	1.13	0.23	27	6	6.0	0.003
4.2	0.5	0.5	0.5	0.80	0.07	8	6	7.5	0.003
4.2	0.5	0.5	0.25	0.56	0.05	5	7	9.0	0.003
4.2	1.0	1.0	1.0	0.80	0.19	27	3	5.0	0.005
4.2	1.0	1.0	0.5	0.56	0.09	9	7	6.5	0.005
4.2	1.0	1.0	0.25	0.40	0.06	6	9	8.0	0.005
4.2	3.0	3.0	1.0	0.46	0.25	16	7	4.5	0.01
4.2	3.0	3.0	0.5	0.33	0.15	9	7	5.5	0.01
4.2	3.0	3.0	0.25	0.23	0.11	6	11	7.0	0.01
0.9	1.0	1.0	1.00	0.80	0.60	57	1.1	2.0	0.001
0.45	1.0	1.0	1.00	0.80	1.20	80	0.6	1.5	0.001

achieve a photon power per Hz of about $2h\nu$, using junctions with a critical current density of 10^8 Am^{-2}. Junctions with a smaller area and a higher critical current density should enable one to achieve an even better performance, provided that heating or other nonequilibrium effects do not become important. The near-ideal performance for a given bias current is obtained over a relatively narrow range of flux, typically 10^{-3}-$10^{-2}\Phi_o$. However, since the flux noise is typically 10^{-8} $\Phi_o Hz^{-1/2}$, the dynamic range of the amplifier can still be considerable, at least 10^5 in a unit bandwidth. The limited working range of the SQUID makes it most attractive as a small-signal amplifier, without flux modulation or negative feedback, although operation in a flux-locked loop with near-ideal sensitivity may not be out of the question. In our calculations we have entirely neglected the contributions of 1/f noise which will, of course, degrade the performance at low frequencies. On the other hand, the quoted performance should be obtainable up to high frequencies, say 1/10 of the Josephson frequency or about 10 GHz for the devices listed in Table 4.1.

We also remark that it may be difficult to achieve a high coupling coefficient α between a SQUID with an inductance as low as 1pH and an input inductance large anough to be useful in many applications. In principle, since α does not appear in Eq. (4.6), a low coupling efficiency does not have a deleterious effect on the noise temperature, but, in practice, a low value of α may lead to undesirable values of R_i and/or C_i (Tesche and Clarke; 79). However if one were to reduce the junction area to 0.1 μm^2, one could increase L to the more useful

value of 100 pH and still achieve comparable performances to those listed in Table 4.1.

V. DC SQUID MEASUREMENTS

Recently, there have been substantial improvements in the sensitivity of dc Superconducting QUantum Interference Devices (SQUIDs). Generally, the performances have been in reasonable agreement with the prediction for an optimized SQUID, (Tesche and Clarke, 77) $\varepsilon/1\text{Hz} \equiv S_\Phi/2L \approx 10\ k_B T(LC)^{1/2}$ (for $\Gamma \equiv 2\pi k_B T/I_o\Phi_o = 0.05$), where $\varepsilon/1$ Hz is the flux noise energy. Here, S_Φ is the spectral density of the equivalent flux noise of a SQUID of inductance L, and C is the capacitance of each of the Josephson tunnel junctions. This result assumes that the flux noise arises from thermal noise in the resistors shunting the junctions. The lowest noise energy reported so far, approximately $6\hbar$, has been achieved by Voss et al. (1981) and by Cromar and Carelli (1981). In Section IV we computed the noise energy when quantum corrections to the noise generated in the shunts near the Josephson frequency, ν_J, become important. This noise is mixed down to the measurement frequency ($\ll\nu_J$) by the non-linearity of the junctions. In the limit T = 0, the noise in the shunts reduces to zero point fluctuations, and the limiting noise energy is $\varepsilon/1\ \text{Hz} \simeq \hbar$. In this section, we report measured noise energies of dc SQUIDs in the 1 to 4.2K temperature range that, after subtraction of a 1/f component, are within a factor of two of the theoretical limit for T = 0. These measurements were done primarily by Professor Dale Van Harlingen.

1. Experimental Procedures

The SQUIDs were designed to have very low values of L and C and the optimized values $\beta \equiv 2LI_o/\Phi_o \approx 1$ and $\beta_c \equiv 2\ I_o R^2 C/\Phi_o \approx 1$, where I_o and R are the critical current and shunt resistance of each junction,

and Φ_o is the flux quantum. The configuration is shown inset in Fig. 5.2, and is similar to that used by Cromar and Carelli. Two Pb(20 wt. % In) - In_2O_3 - Pb tunnel junctions of nominal diameter 2 μm and separation 30 μm were defined by lifting off windows in an SiO insulating layer. Additional windows determine the length of a 10 μm-wide CuAl resistive shunt for each junction. The capacitance of each junction is estimated to be 0.3 pF, while the SQUID loop, consisting of the insulating layer separating the upper and lower electrodes, has a self-inductance of about 2 pH. The SQUID inductance, L, was estimated in two ways. In the first, we measured the mutual inductance with respect to a current along the counter electrode, and assumed this value to be L/2. In the second, we measured the maximum and minimum critical currents, and estimated β from Fig. 4 of Tesche and Clarke (1977). The two methods agreed to within 4% and 7% for SQUIDs A and B. We have used the first method to obtain the values quoted in the tables. We did not measure C and R directly, and the errors in the quoted values may be as high as $\pm$50%. The SQUID may be flux-modulated by passing a current along the counter-electrode.

Figure 5.1(a) shows the voltage, V, vs. the applied flux, Φ, for a typical SQUID. The structure on the V-Φ characteristic arises from resonances excited when the Josephson frequency is a subharmonic of the LC-resonance frequency. Figure 5.1(b) shows $\partial V/\partial\Phi$ and the dynamic resistance $R_D = \partial V/\partial I$ vs. Φ. Both quantities show sharp peaks when the bias current is just above the critical current. This sharp response and the large values of $\partial V/\partial\Phi$ and R_D are obtained because the noise-rounding in the I-V and V-Φ characteristics is rather small for

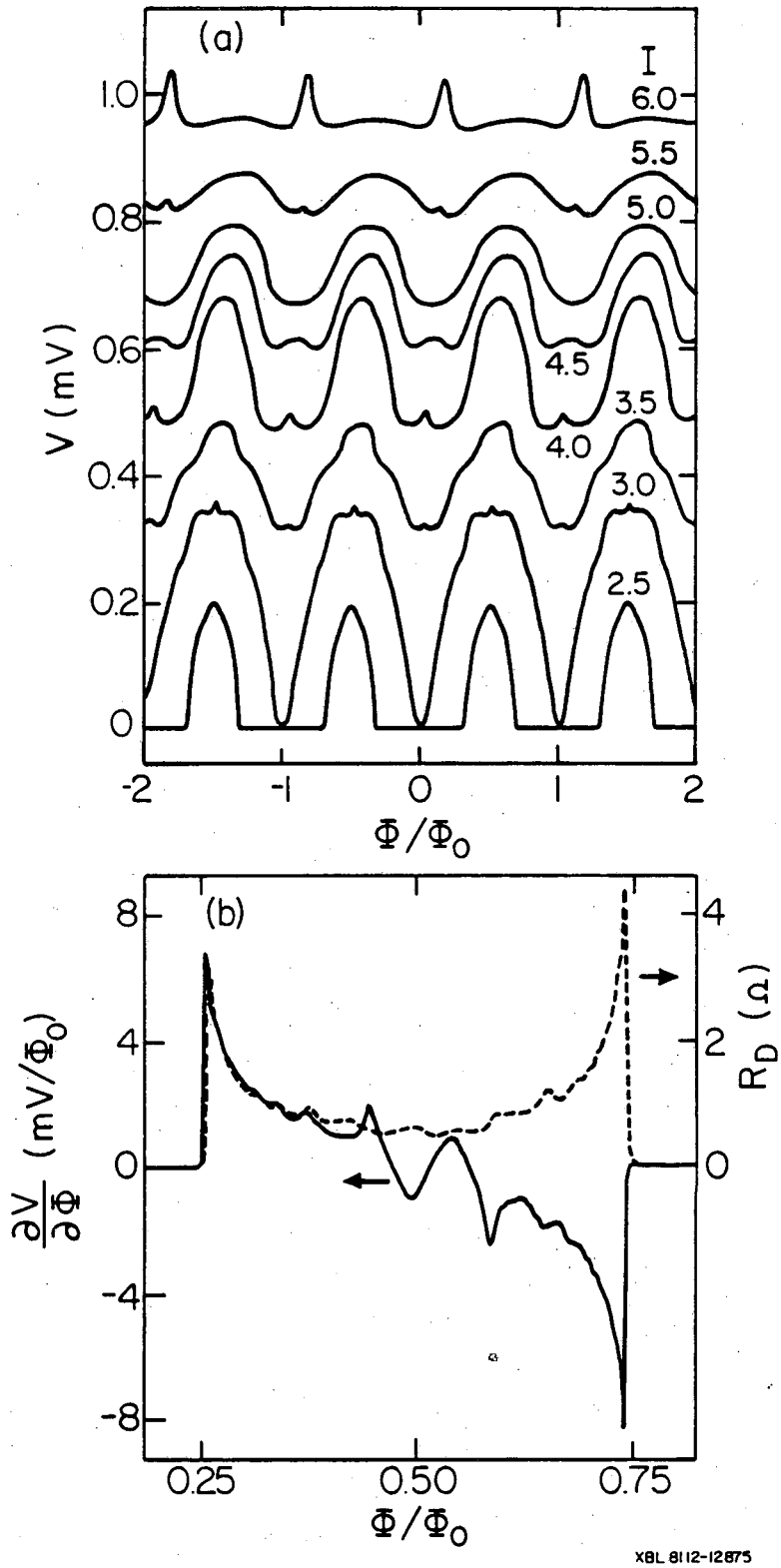

Fig. 5.1 (a) Voltage-flux characteristics for a typical SQUID at 4.2K for 8 values of bias current; (b) transfer function $\partial V/\partial \Phi$ (solid line), and dynamic resistance, R_D (dashed line), vs. Φ/Φ_o for the SQUID in (a) at 4.2K with I = 2.70 mA.

the high critical current junctions used. It is interesting to note that $\partial V/\partial\Phi$ scales almost exactly with R_D when $\partial V/\partial\Phi$ exceeds about 1.5 mV/Φ_o.

To measure the spectral density of the voltage noise, S_V, we coupled the SQUID to a low-noise preamplifier via one of two cooled LC-tank circuits. By connecting the two tank circuits together at the top of the cryostat we obtained an intermediate resonant frequency. The noise at each measurement frequency was mixed down to frequencies below 1kHz, and the low-frequency spectral density was measured with a computer. The gain of the preamplifier-mixer-computer chain was calibrated against the thermal noise of a resistor at the preamplifier input. The preamplifier noise temperature, about 2.8K, was negligible compared with the effective output temperature of the SQUID, $S_V/4k_BR_D$, which was typically 70K. The noise contributed by the tank circuits separately was negligible, but the noise of the combined tank circuit, which contained leads at room temperature, was typically 10% of the SQUID noise, and was subtracted from the total measured noise. We measured $\partial V/\partial\Phi$ by applying a 1 kHz flux with an amplitude of 10^{-4} Φ_o or less, and measuring the voltage across the SQUID with a lock-in detector. We then computed $S_\Phi = S_V/(\partial V/\partial\Phi)^2$.

This technique for measuring S_Φ can lead to substantial errors if the I-V characteristic is slightly hysteretic, because one can obtain an artificially high value of $\partial V/\partial\Phi$. To guard against this problem, we applied a very small flux noise (comparable to the intrinsic flux noise) to the SQUID at the measurement frequency, and observed the increase in the voltage noise. For SQUIDs with large values of $\partial V/\partial\Phi$,

we were able to measure S_Φ directly in this way, obtaining values that were within $\pm 30\%$ of those obtained by the alternative method. However, for small values of $\partial V/\partial\Phi$, where it was necessary to apply a larger amplitude of flux noise to produce an observable effect, there was significant inductive coupling of the noise to the leads attached to the SQUID. In this case, the method could not be used to measure S_Φ, but could still be used to check for the absence of hysteresis.

2. Results

We report here on only two of several SQUIDs studied, with parameters given in Tables 5.1 and 5.2. For both SQUIDs, the critical current increased by about 20% when the temperature was lowered to 1.4K. In addition, both the maximum value of $\partial V/\partial\Phi$ and R_D increased as the temperature was lowered, largely as a result of the reduction in the noise rounding of the I-V characteristic. The characteristic of SQUID B became hysteretic at about 3K, so that data could not be obtained at temperatures much below 3.4K.

The measured values of ε/1 Hz vs. T for SQUID A are shown in Fig. 5.2. The noise at each measurement frequency decreases roughly linearly as T is lowered. We estimate the accuracy of each point to be $\pm 5\%$. The lowest measured value of ε/1 Hz obtained at 1.4K and 202 kHz was $3.2 \pm 0.2\hbar$, corresponding to an equivalent flux noise of $S^{1/2} = (1.7 \pm 0.1) \times 10^{-8}\ \Phi_o\ \mathrm{Hz}^{-1/2}$. It is evident from Fig. 5.2 that there exists a substantial frequency-dependent contribution to the SQUID noise. From noise measurements at the three frequencies we determined that the spectral density of the excess noise exhibited

Table 5.1. Performance of SQUID A (At 4.2K, L = 1.9 pH, C ≈ 0.3 pF, I_o = 0.55 mA, R ≈ 1.3Ω, β = 1.0, β_c ≈ 0.9).

T	∂V/∂Φ	R_D	ε/1Hz (ħ)				
(K)	(mV/Φ_o)	(Ω)	220kHz	149kHz	112kHz	white	1/f (100kHz)
4.2	6.8	4.7	14.4	18.2	23.2	3.6 ± 3.0	21.6 ± 4.7
2.8	9.4	6.4	8.6	10.6	13.2	2.8 ± 1.8	11.6 ± 28
1.8	12.5	8.9	4.5	--	6.9	1.5 ± 1.0[a]	6.0 ± 1.5
1.4	13.9	11.1	3.2	4.0	5.1	0.8 ± 0.7	4.8 ± 1.0

Table 5.2. Performance of SQUID B (At 4.2K, L = 2.5 pH, C ≈ 0.3 pF, I_o = 0.38 mA, R ≈ 1.6Ω, β = 0.9, β_c ≈ 0.9)

T	∂V/∂Φ	R_D	ε/1Hz (ħ)			
(K)	(mV/Φ_o)	(Ω)	118kHz	34kHz	white[a]	1/f[a] (100kHz)
4.2	6.5	3.2	5.2	11.5	2.7 ± 0.6	3.0 ± 0.4
3.8	11.3	4.5	4.5	10.6	2.1 ± 0.5	2.7 ± 0.4
3.4	22.0	7.7	3.7	8.7	1.7 ± 0.4	2.3 ± 0.3

[a]Measurements made at two frequencies only: Excess noise is assumed to scale as 1/f.

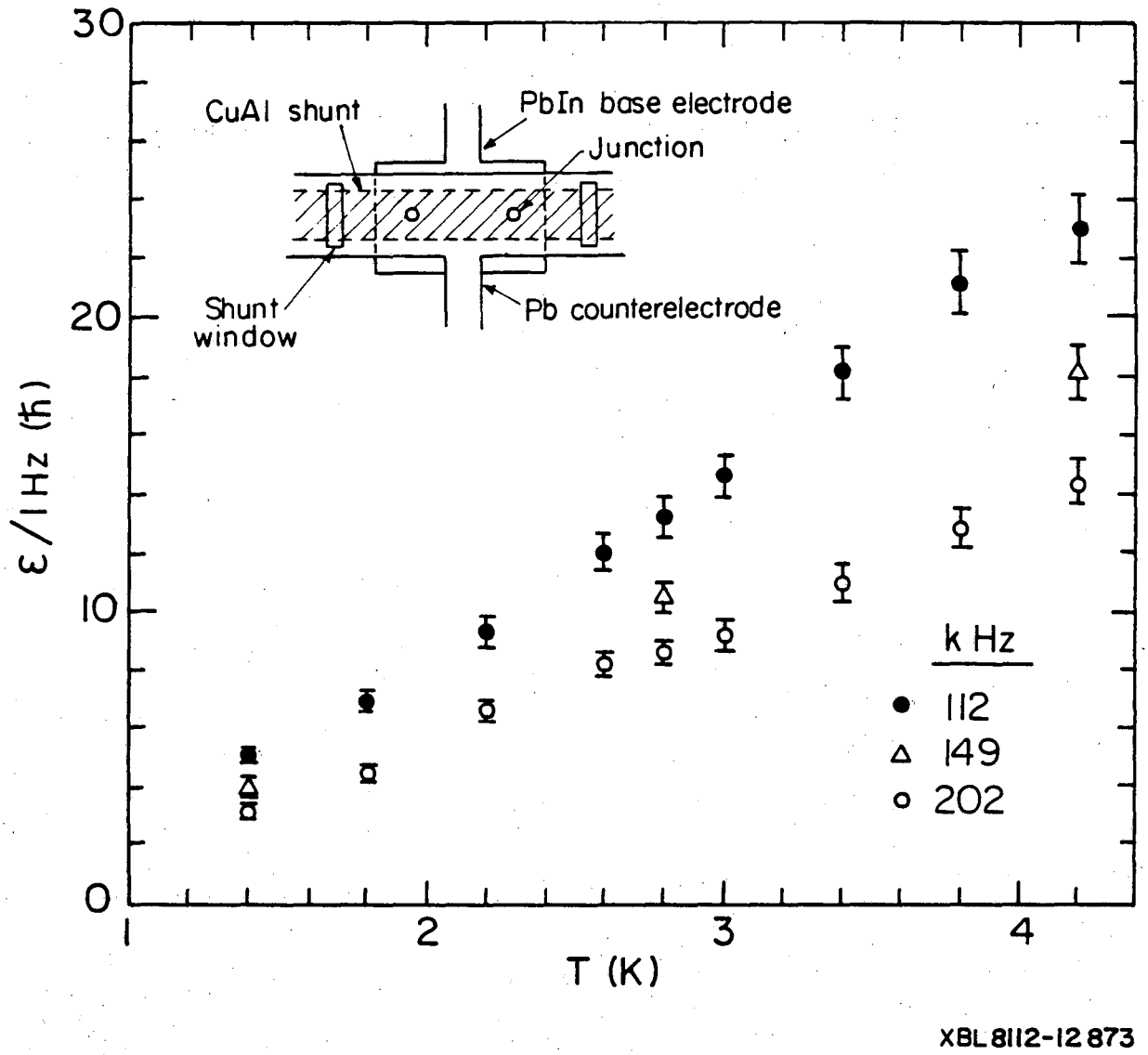

Fig. 5.2 Measured ε/1 Hz vs. T at three frequencies for SQUID A, with ± 5% error bars. Inset shows SQUID configuration.

a power law variation close to 1/f. This conclusion is supported by low frequency measurements which show ε/1 Hz scaling accurately at 1/f over four decades of frequency between 0.1 and 1000 Hz. The measured magnitude of the 1/f contribution below 1 kHz agrees with the value extrapolated from the high frequency data to within 20%. The measured noise can thus be resolved into white noise and 1/f noise components, with the values listed in Table 5.1.

In Fig. 5.3, we plot ε/1 Hz (including 1/f noise) vs. Φ for SQUID A. Although $\partial\nu/\partial\Phi$ is sharply peaked in Φ, with a peak width less than 10^{-3} Φ_o, we see ε/1 Hz is roughly constant for a range of order 0.1 Φ_o. This result is expected since S_Φ varies as $R_D^2/(\partial V/\partial\Phi)^2$, and R_D scales closely with $\partial V/\partial\Phi$ [Fig. 5.1(b)]. Thus, although we have not attempted to do so, it should be possible to operate these SQUIDs in a flux-locked loop without significant loss of sensitivity.

Data for SQUID B were obtained only at two frequencies, 34 kHz and 118 kHz, so that we had to assume that the spectral density of the excess noise was proportional to 1/f. For this SQUID, the magnitudes of the white noise and 1/f noise at 100 kHz were comparable. The lowest observed noise energy was $(3.7 \pm 0.2)\hbar$ at 118 kHz and 3.4K, a value that yields a white noise energy of $(1.7 \pm 0.4)\hbar$.

3. Concluding Remarks

Given the substantial errors, the measured values of the white noise energy for both SQUIDs are in reasonable agreement with the predictions. For a device with $L \approx 2$ pH, $C \approx 0.3$ pF, $\beta_c \approx 1$, and $\beta \approx 1$ we expect ε/1 Hz to be about $3\hbar$ at 4.2K, decreasing to a little more

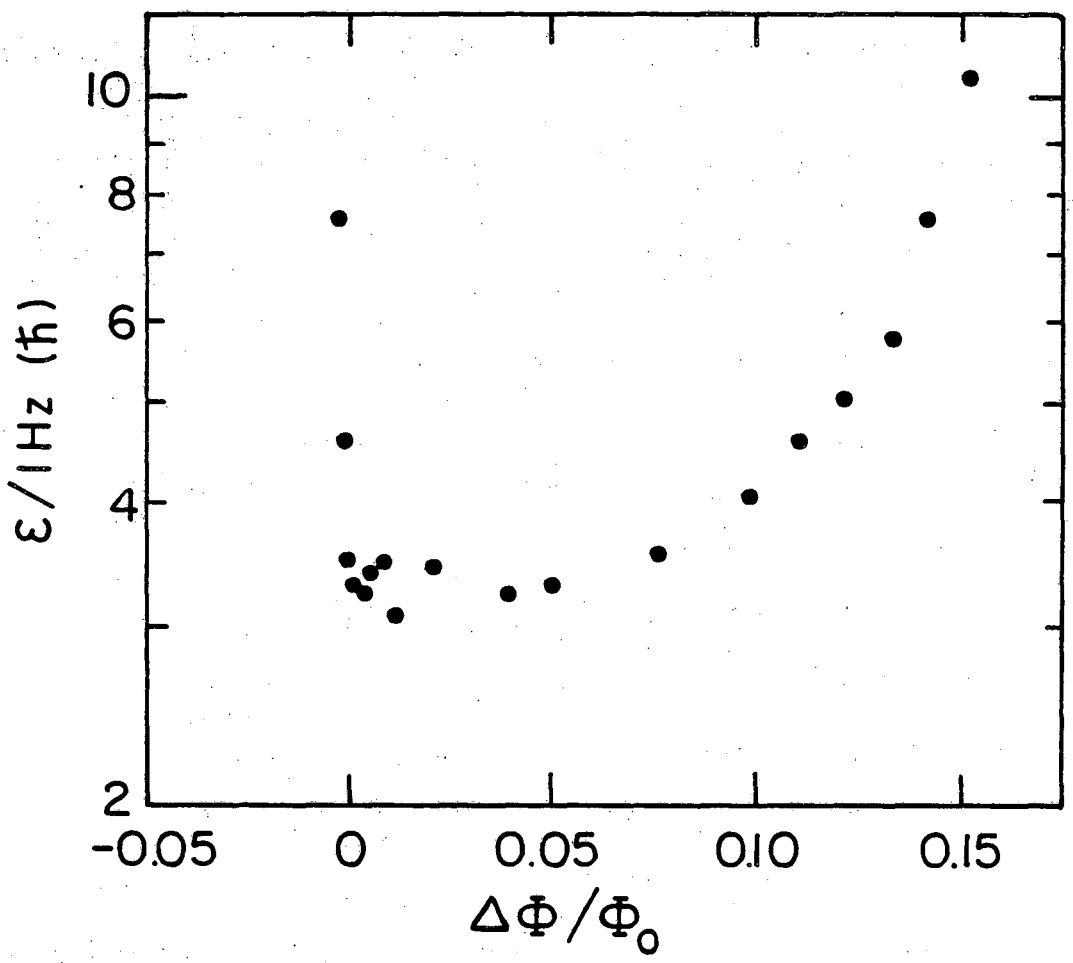

XBL8112-12872

Fig. 5.3 Measured $\varepsilon/1$ Hz vs. $\Delta\Phi/\Phi_0$ for SQUID A at 202 kHz and 1.4K. $\Delta\Phi$ is measured relative to the flux for which $\partial V/\partial\Phi$ is a maximum.

than $\hbar$ at 1K. We believe that the best measured white noise energy at 1.4K was below $2\hbar$, but, given the large error bars, we cannot determine whether or not the noise was beginning to level off as the temperature was lowered. I personally believe the SQUID had reached the "quantum limit".

The present series of SQUIDs is not appropriate for quasistatic or low frequency measurements in view of the high level of 1/f noise and very small in input inductance. However, they may be useful as high frequency amplifiers, in a stripline configuration. Since the Josephson frequency at the operating voltage is typically 25 GHz, one might expect the high sensitivity to extend to frequencies of at least several GHz.

APPENDIX A.

TWO METHODS OF COMPUTING I-V CHARACTERISTICS AND NOISE IN RESISTIVELY SHUNTED JUNCTIONS

In this appendix, we outline two methods of computing the I-V characteristics and spectral density of the voltage noise for resistively shunted junctions. The first method calculates the I-V characteristics and R_D, including noise-rounding, and can also be used to compute the spectral density of the voltage noise, although the last calculation is rather slow. Unfortunately, for reasons that we will explain, this method is not useful for computing the noise in a junction with resonant structure, such as junction 4. The second method calculates the noise very efficiently at voltages where noise rounding is negligible. With the model of the junction we have used, this method appears to account for most of the data observed on junction 4 satisfactorily, although higher order corrections might provide a better fit at voltages above, say 500 μV.

Method 1

The model circuit, inset in Fig. 3.9 is described by Eqs. (3.3) and (3.4). We rewrite these equations in dimensionless units $v = V/I_oR$, $i = I/I_o$, $s = I_s/I_o$, and $\theta = t/(\Phi_o/2\pi I_oR)$, and use ω as a dimensionless angular frequency to obtain:

$$i = \sin\delta + \beta_c\ddot{\delta} + s \tag{A1}$$

and

$$\dot{\delta} = s + \beta_L\dot{s} + v_n \ , \tag{A2}$$

where $\dot{\delta} \equiv \partial\delta/\partial\theta$, etc., and we have used $2eV = \hbar\partial\delta/\partial t$. As usual, $\beta_c \equiv 2\pi I_o R^2 C/\Phi_o$ and $\beta_L \equiv 2\pi L_s I_o/\Phi_o$. The instantaneous state of the junction is specified completely by $\dot{\delta}$, δ and s. Using Eqs. (A1) and (A2) one can compute $\dot{s}$ and $\ddot{\delta}$ and the higher order derivatives of δ and s, for example:

$$\beta_L \ddot{s} = \ddot{\delta} - \dot{s} \ , \tag{A3}$$

$$\beta_c \dddot{\delta} = - \dot{\delta} \cos\delta - \dot{s} \ , \tag{A4}$$

and so on. We have neglected all derivatives of v_n. Once the derivatives have been evaluated numerically for the existing values of δ, $\dot{\delta}$, and s at time θ, we compute the new values of δ_1, $\dot{\delta}_1$, and s_1 at a later time, $\theta + \tau$, by using a fifth-order Taylor expansion:

$$\delta_1 = \delta + \dot{\delta}\tau + \ldots + (\partial^5\delta/\partial\theta^5)\tau^5/5! \ , \tag{A5}$$

$$\dot{\delta}_1 = \dot{\delta} + \ddot{\delta}\tau + \ldots + (\partial^5\delta/\partial\theta^5)\tau^4/4! \ , \tag{A6}$$

and

$$s_1 = s + \dot{s}\tau + \ldots + (\partial^5 s/\partial\theta^5)\tau^5/5! \ . \tag{A7}$$

To predict the average voltage for $i > 1$, we set $v_n = 0$, integrate Eqs. (A1) and (A2) numerically over exactly one Josephson cycle, measure the required time θ, and compute $\langle v \rangle = \langle \dot{\delta} \rangle = 2\pi/\theta$. This procedure was used to compute the values of R_D in Fig. 3.9, with values of L_s and C chosen to fit the data.

The results were independent of the length of the time step, τ, provided τ was less than the smaller of β_c or β_L. To check that the

presence of noise did not affect the characteristics for $i > 1$, we varied v_n in time to simulate noise from the resistor while the junction was allowed to evolve over many Josephson cycles. The resulting values of the voltage were identical to those with $v_n = 0$.

To obtain a time-representation of $v_n(\theta)$ with a white power spectrum, $S_v^w(\omega)$, we used a pseudorandom number generator to produce voltage pulses that were gaussian distributed in amplitude and uncorrelated in time. A non-white power spectrum, $S_n^{nw}(\omega)$, could be generated, when necessary, by convolving this time representation with an appropriate filter function. This filter function was chosen so that its transfer function in the frequency domain, $T(\omega)$, satisfied

$$S_v^{nw}(\omega) = |T(\omega)|^2 S_v^w(\omega). \tag{A8}$$

The high-frequency cut-off, ω_H, of $v_n(\theta)$ was always chosen to be large enough that the predicted average voltage and noise voltage were independent of the value of ω_H when the latter was varied over a factor of 20 or more. Furthermore, when the noise near the Josephson frequency was non-white, we took account of the implied non-zero correlation time by ensuring that the correlation time of the filter was much larger than $1/\nu_J$.

To obtain $\langle\dot{\delta}\rangle$, the computed values of $\dot{\delta}(\theta)$ were filtered with a low-pass gaussian filter with a roll-off frequency, ω_L, of 0.03 to 0.1 ω_J. The fluctuations in the filtered values of $\langle\dot{\delta}\rangle$ were used to compute the low frequency spectral density of the voltage noise. This spectral density was independent of the roll-off frequency of this low-pass filter.

This method was used to predict $\langle\dot{\delta}\rangle$ and the fluctuations in $\dot{\delta}$ in single junctions and dc SQUIDs, including low-voltage regions of the I-V characteristics where there is significant noise rounding. However, when we tried to use this method to predict the noise in junction 4, which has substantial resonant structure, we obtained very poor results. The essential problem was that the resonant frequency, $\omega_{LC} = (L_s C)^{-1/2}$, was typically 5 to 20 times higher than ω_J, while ω_H was necessarily at least several times greater than ω_{LC}. Thus, since ω_L was typically an order of magnitude less than ω_J the ratio of ω_H/ω_L was typically 10^3. Consequently, the ratio of the "input" noise power to the "output" noise power for "f-noise" was typically 10^6. The computed spectral densities of the noise proved to be erratic with such large ratios, possibly because of our neglect of the derivatives of v_n in Eq. (A3). As a result, we had to abandon this technique for junctions with resonant structure.

Method 2

Above the noise-rounded region of the I-V characteristic, we used a more accurate but more complicated method to calculate the noise in resonant junctions. In this region, following the perturbation approach of Likharev and Semenov (1972), we can expand δ and s:

$$\delta(\theta) = \delta_o(\theta) + \tilde{\delta}(\theta) \tag{A9}$$

and

$$s(\theta) = s_o(\theta) + \tilde{s}(\theta) \ , \tag{A10}$$

where δ_o and s_o are the noise-free solutions for the phase and shunt current, and $\tilde{\delta}$ and $\tilde{s}$ represent small departures from δ_o and s_o due to noise. Substituting these exprssions into Eqs. (A1) and (A2), we find

$$0 = \tilde{\delta}\cos\delta_o + \beta_c\ddot{\tilde{\delta}} + \tilde{s} \tag{A11}$$

and

$$\dot{\tilde{\delta}} = \tilde{s} + \beta_L\dot{\tilde{s}} + v_n \tag{A12}$$

We Fourier transform these equations over the range $-\infty < \omega < \infty$ to obtain

$$0 = \int_{-\infty}^{\infty} F(\omega')\tilde{\delta}(\omega - \omega')d\omega' + \beta_c(-\omega^2)\tilde{\delta}(\omega) + \tilde{s}(\omega) \tag{A13}$$

and

$$j\omega\tilde{\delta}(\omega) = (1+j\omega\beta_L)\tilde{s}(\omega) + v_n(\omega) \ , \tag{A14}$$

where $F(\omega')$ is the normalized Fourier transform of $\cos\delta_o(\theta)$. Since $\cos\delta_o(\theta)$ is a periodic function, $F(\omega')$ consists of a series of spiked functions centered at $\omega = 0$ and spaced at intervals of ω_J. Setting $\omega' = k\omega_J$, where k is an integer, we can transform the integral to a sum, replace $F(k\omega_J)$ with F_k, and eliminate s between Eqs. (A13) and (A14) to find

$$\sum_{k=-\infty}^{\infty} F_k\tilde{\delta}(\omega - k\omega_J) + \left(\frac{j\omega}{1 + j\omega\beta_L} - \omega^2\beta_c\right)\tilde{\delta}(\omega) = \frac{v_n(\omega)}{1 + j\omega\beta_L} \ . \tag{A15}$$

In subsequent calculations, we have shown that there exists a maximum value of $|k|$, k_m, above which the noise at frequency $k\omega_J$ is not significantly mixed down to the measurement frequency. Cutting off the summation at $\pm k_m$, we are left with $2k_m + 1$ inhomogeneous equations with unknown phases $\tilde{\delta}(\omega - \ell_m\omega_J)$, ..., $\tilde{\delta}(\omega + \ell_m\omega_J)$, where $|\ell| \leqslant k_m$. To solve these, we first compute the coefficients F_k using method 1 (with $v_n = 0$). The required fluctuations in the $\tilde{\delta}(\omega - \ell\omega_J)$ are then obtained by a conventional matrix inversion of Eq. (A15). We find

$$\tilde{\delta}(\omega + \ell\omega_J) = \sum_{k=-k_m}^{+k_m} \frac{A_{\ell,k}\, v_n(\omega + k\omega_J)}{1 + j(\omega + k\omega_J)\beta_L} \quad , \tag{A16}$$

where $\bar{\bar{A}} \equiv \bar{\bar{B}}^{-1}$, and $\bar{\bar{B}}$ is the matrix representation of Eq. (A15):

$$\{\bar{\bar{B}}\}_{\ell,k} = F_{\ell-k} + \delta_{\ell,k}\left[\frac{j(\omega + \ell\omega_J)}{1 + j(\omega + \ell\omega_J)\beta_L} - (\omega + \ell\omega_J)^2\beta_c\right] \quad . \tag{A17}$$

In Eq. (A17), $\delta_{\ell,k}$ is the Kronecker delta. Since the v_n at different frequencies are independent, the noise at the measurement frequency can be obtained from Eq. (A16) with $|\omega| << |\omega_J|$ and $\ell = 0$:

$$S_{\dot{\delta}}(\omega) = \sum_{k=-k_m}^{k_m} |z_k(\omega)|^2 S_i(\omega + k\omega_J) \quad , \tag{A18}$$

where

$$z_k(\omega + \ell\omega_J) = \frac{j(\omega + \ell\omega_J)A_{\ell,k}}{1 + j(\omega + k\omega_J)\beta_L} \quad , \tag{A19}$$

is the complex dimensionless impedance that mixes noise from $(\omega + k\omega_J)$ to $(\omega + \ell\omega_J)$, and $S_i\ (\omega + k\omega_J)$ is the dimensionless spectral density of the noise current in the resistor. We obtain Eq. (3.7) from Eq. (A18) by replacing ω with ν, setting $\nu = 0$, using positive frequencies only, and assigning appropriate dimensions. In dimensioned units, at frequencies small compared with Z_o/L_s, Z_o is just the dynamic resistance. Thus, the method can be tested by comparing the value of Z_o with the value of R_D obtained with method 1. The computed values of $Z(\omega)$ were shown to be independent of ω for $\omega \ll \omega_J$, and ω/ω_J was chosen to be between 1/30 and 1/10. The value of k_m, typically 16 to 25, was chosen so that $k_m\omega_J \gg \omega_{LC}$; the value of k_m was varied to show that the values of $Z(\omega)$ did not depend on it.

The method was used to compute the spectral density of junction 4 shown in Fig. 3.11, and the corresponding values of $|Z_k|^2$ in Fig. 3.12. The complexity of the method does not easily allow the value of R to be voltage dependent, and the noise in Fig. 3.11 was computed with $R = 0.092\Omega$ for all voltages. This approximation gave rise to the discrepancy between the measured and predicted noise at low voltages in Fig. 3.11.

APPENDIX B. NOISE IN TIGHTLY COUPLED SQUIDS

We wish to analyze the problem of a SQUID tightly coupled to an input coil. The appendix was motivated by C. Tesche (1982) who first worked out the problem incorrectly in a different way. The effect of the input circuit shown in Fig. (4.2) can be added to the SQUID equations (4.1) to (4.4) with the change that equation (4.1) becomes

$$\Phi(\omega) - \frac{\Phi_o}{2\pi}(\dot{\delta}_1 - \delta_2) + L\,J(\omega) - \frac{j\omega M^2 J(\omega)}{Z + j\omega L_i} = 0 \tag{B1}$$

where Z is the impedence of the input circuit excluding the input coil and the reflected SQUID impedence, and we have set $V_i = 0$. We now add an additional flux source in the SQUID loop only with a spectral amplitude

$$\Phi^v(\omega) = -\alpha^2 LJ(\omega) + \frac{j\omega M^2 J(\omega)}{Z + j\omega L_i} \tag{B2}$$

this source exactly cancels the effect of the input circuit and effectively reduces the self-inductance of the SQUID from L to $L(1-\alpha^2)$. Now solve the SQUID equation for the bare SQUID with the reduced inductance, and call the results S_V^{bare}, S_J^{bare}, $\bar{V}^{bare}$, etc. Now $\Phi^v(\omega \geqslant \omega_J) = 0$, provided $|Z| << \omega_J L_i$ which is usually true, which means we can remove the additional flux source at high frequencies ($\omega \geqslant \omega_J$) leaving everything unchanged. Secondly removing the additional source at low frequencies has two effects: (1) the input circuit source $-\omega^2 M^2 J(\omega)/(Z + j\omega L_i)$ is restored and (2) we have an effective flux source in the SQUID $\Phi^e(\omega) = \alpha^2 LJ(\omega)$ at low frequencies ($\omega << \omega_J$). The resulting output

noise from this source can be analyzed linearly because it's only non-zero at low frequencies. Hence when $\omega << \omega_J$

$$V(\omega) = V(\omega)^{bare} + (\partial V/\partial\Phi)\ \alpha^2\ LJ(\omega)^{bare} \tag{B3}$$

$$J(\omega) = J(\omega)^{bare}\ (1 + \alpha^2 L/L_c) \tag{B4}$$

where

$$\frac{1}{L_c} = \frac{1}{L_D} + \frac{j\omega}{R_c} \tag{B5}$$

and $L_D \equiv \Delta\Phi_a/\Delta\bar{J}$ and R_c is the lossy part of this response (see the end of this appendix). We find

$$S_V^o = S_V^{o,bare} + \left(\frac{\partial V}{\partial\Phi}\right)^2 \alpha^4 L^2 S_J^{o,bare} + 2\left(\frac{\partial V}{\partial\Phi}\right) \alpha^2 L\ S_{VJ}^{o,bare} \tag{B6}$$

$$S_J^o = S_J^{o,bare}\ |1 + \alpha^2 L/L_c|^2 \tag{B7}$$

$$\bar{\Phi} = \bar{\Phi}^{bare} - \alpha^2 L\bar{J} \tag{B8}$$

The first order current source in the input circuit from the SQUID is $-j\omega MJ/(Z + j\omega L_i)$, but we need to consider the second order current source in the input circuit, which is the extra current source in the input from the change in flux in the SQUID introduced by the first order current source in the input, this is:

$$-\left\{j\omega MJ/(Z + j\omega L_i)\right\} \cdot \left\{j\omega M^2/((Z + j\omega L_i)L_c)\right\} .$$

Adding all orders of current noise in the input we have

$$I_{total} = \frac{-j\omega MJ}{(Z + j\omega L_i)} \left\{ 1 + \frac{j\omega M^2}{(Z + j\omega L_i)L_c} + \left(\frac{j\omega M^2}{(Z + j\omega L_i)L_c} \right)^2 + \ldots \right\} =$$

$$\frac{-j\omega MJ}{(Z + j\omega L_i)} \sum_{n=o}^{\infty} \left(\frac{j\omega M^2}{(Z + j\omega L_i)L_c} \right)^n = \tag{B9}$$

$$\frac{-j\omega MJ}{(Z + j\omega L_i)} \left\{ \frac{1}{1 - \frac{j\omega M^2}{(Z + j\omega L_i)L_c}} \right\} = \frac{-j\omega MJ}{Z + j\omega L_i - \frac{j\omega M^2}{L_c}}$$

The reason for doing this is because we are not solving directly the equation of motion for the tightly coupled SQUID, but only treating the input as a perturbation; hence we must take the total effect of the input into consideration. The effect can be visualized as a reflected SQUID impedence of:

$$Z_R = -j\omega M^2/L_c = -j\omega M^2 \ (1/L_D + j\omega/R_c) \ . \tag{B10}$$

The values of L_D and R_c, the dynamic low-frequency inductance and resistance to an applied flux will depend on the SQUID bias point and the SQUID readout system ($R_c = O(L_D R/L)$ for normal SQUID operation). Clarke, Tesche, and Giffard (1979) (CTG) used $\omega^2 M^2/4R_D$ for the reflected SQUID impedence, where they should have used Z_R. Also their equation 7 has the wrong sign for the current noise term, hence the sign of γ_{VJ} needs to be taken as negative in the remainder of the paper.

The formalism in CTG may be used in the large-α^2 limit by simply changing from the bare values of L, S_V, S_J, etc. to the tightly coupled values and making the change to the proper value of the reflected SQUID impedence, Z_R. In the small-α^2 limit, CTG is unchanged as expected. This approach to the tightly coupled SQUID should be good as long as the input circuit looks inductive at the Josephson frequency or higher.

APPENDIX C

MACROSCOPIC QUANTUM EFFECTS

Appendix C concerns itself with converting the microscopic Hamiltonian picture of a shunted current-biased Josephson junction to the macroscopic 'cos δ' potential. In this way the microscopic meaning and existence of macroscopic quantum effects in Josephson junctions can be clearly interpreted.

Lets start with the Hamiltonian for the junction without a bias current or resistor added. It is simply:

$$H_J = \frac{e^2}{2C}(n_R - n_L)^2 + (H_T^+ + H_T^-). \tag{C1}$$

Here $n_R(n_L)$ is the number operator for pairs on the right (left) side of the junction, C is the junction capacitance, and $H_T^-(H_T^+)$ transfers a pair across the junction from right to left (left to right). H_T^+ can be represented as

$$H_T^+ = \frac{-E_J}{2N} a_R^+ a_L \tag{C2}$$

where N is the total number of pairs, E_J is the tunnelling energy and a_R^+ creates a pair on the right side, etc. The basis states used to represent the system are pair number states

$$|m\rangle \equiv |N + m\rangle_R |N - m\rangle_L. \tag{C3}$$

N is very large so we have $-N \ll m \ll N$, for any of the physically import-

ant excited states ($m \neq 0$).

The eigenenergies are calculated by writing the eigenfunctions as linear combinations of the $|m\rangle$ states

$$|\psi_\ell\rangle = \sum_m b_m^\ell |m\rangle. \tag{C4}$$

The Schrödinger equation for an eigenstate, operated on by the bra $\langle n|$ from the left:

$$\langle n|\varepsilon_\ell|\psi_\ell\rangle = \langle n|H_J|\psi_\ell\rangle, \tag{C5}$$

can be evaluated term by term to find the recursion relation for the b_n^ℓ and the eigenenergy for the ℓth state:

$$\varepsilon_\ell b_n = \frac{4e^2n^2}{2C} b_n^\ell - \frac{E_J}{2}(b_{m-1}^\ell + b_{m+1}^\ell). \tag{C6}$$

At this point we could work backward to show this is equivalent to the 'cos δ' Hamiltonian but it is easier to start with the 'cos δ' Hamiltonian and show it leads to the same eigenfunctions with identical eigenenergies. Imagine a particle in a one dimensional potential $-\frac{I_o\Phi_o}{2\pi}\cos x$ with a 'mass' $\frac{C\Phi_o^2}{4\pi^2}$. The Hamiltonian is

$$H_J = \frac{4\pi^2P^2}{2C\Phi_o^2} - \frac{I_o\Phi_o}{2\pi}\cos x \tag{C7}$$

with the commutator

$$[x,P] = i\hbar, \tag{C8}$$

so we have:

$$P = -i\hbar \frac{\partial}{\partial x} . \tag{C9}$$

The units of P are action and x is dimensionless (P will later be proportional to the charge on the capacitor $P = \Phi_o Q/2\pi = \Phi_o CV/2\pi$). The basis states we will expand in to find the eigenstate $\psi_\ell(x)$, are linear combinations of plane waves

$$\psi_\ell(x) = \int_{-\infty}^{\infty} b^\ell(K) e^{iKx} dK. \tag{C10}$$

The Schrödinger equation for ψ_ℓ when multiplied by e^{-iqx} and integrated by x from $-\infty$ to ∞ is: $(-\infty \ll q \ll \infty)$

$$\varepsilon_\ell \int_{-\infty}^{\infty} \psi_\ell(x) e^{-iqx} dx = \int_{-\infty}^{\infty} H_J e^{-iqx} dx. \tag{C11}$$

Again expanding the terms of (C11) term by term one finds that Eq. (C11) now looks like this:

$$\varepsilon_\ell b^\ell(q) = \frac{4e^2 q^2}{2C} b^\ell(q) - \frac{I_o \Phi_o}{2\pi} \left\{ \frac{b^\ell(q-1) + b^\ell(q+1)}{2} \right\} \tag{C12}$$

and it dictates the eigenenergies and expansions in terms of plane waves of the eigenfunctions of the 'cos δ' potential. Notice here that because we have let both x and P run from $-\infty$ to ∞, and not just 0 to ∞ or 0 to 2π etc., there are no problems with the hermicity of x or P and the correctness of the commutator. The eigenfunctions are specified in terms of ℓ (the band index) and the smallest value of q, q_{min}, (the re-

ciprocal lattice vector) in the series of $b^{\ell}(q)$ that are linked together by the $b^{\ell}(q \pm 1)$ terms in Eq. (C12). If when solving the system we only choose initial states whose q_{min} vectors are zero there will be a one to one correspondence between these states and the eigenstates dictated by the microscopic Hamiltonian (C1), because Eq. (C12) with q_{min} equal to zero is the same as (C6) when $I_o\Phi_o/2\pi = E_J$.

Importantly, if we allow a slightly more general wavefunction solution to the micro- and macroscopic junction Hamiltonians:

$$\sum_n b_n|n\rangle \rightarrow \sum_n b_n|n + \alpha\rangle \tag{C13}$$

and

$$\sum_n b_n e^{inx} \rightarrow e^{i\alpha x} \sum_n b_n e^{inx}, \tag{C14}$$

(In Eq. (C14), the solutions are expressed in terms of the basis states, which are greatly reduced for the 'cos δ' Hamiltonian because of the condition for equivalence that $q_{min} = 0$.) we will have a general solution to the system including the bias-current and resistor Hamiltonians. When specifying the initial eigenstate we choose $q_{min} = 0$ and α arbitrarily so the wavefunction magnitude is periodic in 2π and always stays that way.

Since the 'cos δ' Hamiltonian, even with a restricted subset of eigenfunctions, shows tunnelling and it is a different representation of the microscopic Hamiltonian, one could expect tunnelling (MQT) theoretically starting from the macroscopic picture. Since the wavefunction magnitudes are all periodic in 2π, the event of tunnelling cannot be in-

terpreted as the junction phase increasing by 2π, but the voltage across the junction, P, increasing beyond what would otherwise be expected. This is what is actually measured. There is a packet in every well, all packets are created equal, and they stay that way, and tunnelling means they all move downward together. Here we imagine the situation when the $\cos\delta$ potential is tilted by an external bias current. Even in this case, if before applying the bias current the wavefunction magnitude is periodic in 2π, it still will be periodic after the current is applied.

This model of the junction tunnelling predicts interference effects since the probability density entering a well from an uphill well will interfere with that density remaining in the well. At present it is not known if this increases or decreases the average tunnelling rate or not, but this effect could test the "in every well" model presented here.

We now ask for a microscopic picture of macroscopic quantum tunnelling. The junction macroscopic wavefunction $\psi(K)$ consists of many delta functions, since $\psi(x)$ is periodic, and each delta function corresponds in the microscopic picture to a particular number of pairs across the barrier, m. The voltage across the junction, $P = CV\Phi_o/2\pi$, increases because of the tunnelling, which means $\langle\psi|P|\psi\rangle = \hbar\langle\psi|K|\psi\rangle$ is bigger. Macroscopically this just means the amplitudes of these delta functions shift to a higher value of $\overline{K}$ or microscopically that the number of pairs on one side of the junction increases. Its really very simple; put current through the junction, and many pairs move across the junction and some stay across.

The ideal Josephson junction has $\langle\Delta n^2\rangle$ extremely large since the charging energy per pair moving across the junction is vanishingly

small. As $I_oC \to 0$ the charging energy per pair becomes significant forcing the size of $\langle \Delta n^2 \rangle$ to decrease there by increasing $\langle \Delta x^2 \rangle$. Hence we have the broadened wave packet of phase in the macroscopic picture. As $I_oC \to 0$ the response of the pair current for $I < I_o$ goes from the ideal reactive response (the Josephson inductance) to a real and reactive responce, $\overline{V}$ partially in phase with I, to finally a totally real response, i.e., a lack of coherence across the junction.

One should not confuse the tunnelling phenomenon with the effect of tunnelling on an hysteretic junction. The voltage across the junction from the tunnelling means the junction has gained kinetic energy. If the junction is sufficiently under damped, so this energy is not directed to the resistor the system can evolve, possibly with the help of self-interference, into the so-called free running mode.

REFERENCES

V. Ambegoakar and B. I. Halperin, Phys. Rev. Lett. 22, 1364 (1969).

P. W. Anderson, in "Lectures on the Many-Body Problem," edited by E. R. Cainiello (Academic, New York, 1964), Vol. 2 p. 127. (and other places).

A. O. Caldeira and A. J. Leggett, Phys. Rev. Lett. 46, 211 (1981).

H. B. Callen and T. A. Welton, Phys. Rev. 83, 34 (1951).

J. H. Claassen, Y. Taur, and P. L. Richards, Appl. Phys. Lett. 25, 759 (1974).

J. H. Claassen and P. L. Richards, J. Appl. Phys. 49, 4117 (1978).

J. Clarke and G. Hawkins, Phys. Rev. B 14, 2826 (1976).

J. Clarke, C. D. Tesche, and R. P. Giffard, J. Low Temp. Phys. 37, 405 (1979).

M. W. Cromar and P. Carelli, Appl. Phys. Lett. 38, 723 (1981).

A. J. Dahm, A. Denenstein, D. N. Langenberg, W. H. Parker, D. Rogovin, and D. J. Scalapino, Phys. Rev. Lett. 22, 1416 (1969).

C. M. Falco, W. H. Parker, S. E. Trullinger, and P. K. Hansma, Phys. Rev. B 10, 1865 (1974).

R. Ferrell and R. Prange, Phys. Rev. Lett. 10, 479 (1963).

T. A. Fulton, IEEE Trans. Mag. MAG-13, 859 (1977).

The possibility that zero-point fluctuations provided the limiting sensitivity has been discussed by J. C. Gallop and B. W. Petley, J. Phys. E9, 417 (1976).

R. P. Giffard, P. F. Michelson, and R. J. Soulen, IEEE Trans. Magn. MAG-15, 276 (1979).

J. P. Gordon, W. H. Louisell, and L. R. Walker, Phys. Rev. 129, 481 (1963).

J. H. Greiner, C. J. Kircher, S. P. Klepner, S. K. Lahiri, A. J. Warnecke, S. Basavaiah, E. T. Yen, John M. Baker, P. R. Brosious, H.-C. W. Huang, M. Murakami, and I. Ames, IBM J. of Res. and Dev. 24, 195 (1980).

Yu. M. Ivanchenko and L. A. Zil'berman, Zh. Eksp. Teor. Fiz. 55, 2395 (1968) [Sov. Phys. JETP 28, 272 (1969)].

L. D. Jackel, J. P. Gordon, E. L. Hu, R. E. Howard, L. A. Fetter, D. M. Tennant, R. W. Epworth, and J. Kurkijärvi, Phys. Rev. Lett. 47 697 (1981).

J. B. Johnson, Phys. Rev. 32, 97 (1928).

B. D. Josephson, Phys. Lett. 1, 251 (1962).

J. Kurkijärvi and V. Ambegoakar, Phys. Lett. 31A, 314 (1970).

J. Kurkijärvi, Superconducting Quantum Interference Devices and their Applications (Ed. H. D. Hahlbohm and H. Lübbig, Walter de Gruyter, Berlin, 1980), p. 247.

A. J. Leggett, J. de Phys. C6, 1264 (1978).

K. K. Likharev and V. K. Semenov, Pis'ma Zh. Eksp. Teor. Fiz. 15, 625 (1972) [JETP Lett. 15, 442 (1972)].

W. H. Louisell, A. Yariv, and A. E. Siegman, Phys. Rev. 124, 1646 (1961).

D. E. McCumber, J. Appl. Phys. 39, 3113 (1968).

H. Nyquist, Phys. Rev. 32, 110 (1928).

I. R. Senitzky, Phys. Rev. 119, 670 (1960).

R. J. Soulen, Jr. and R. P. Giffard, Appl. Phys. Lett. 32, 770 (1978).

M. J. Stephen, Phys. Rev. 182, 531 (1969).

W. C. Stewart, Appl. Phys. Lett. 12, 277 (1968).

Y. Taur, IEEE Trans. Electron Devices ED-27, 1921 (1980).

C. D. Tesche and J. Clarke, J. Low Temp. Phys. 29, 301 (1977).

C. D. Tesche and J. Clarke, J. Low Temp. Phys. 37, 397 (1979).

C. D. Tesche, J. Low Temp. Phys. 44, 119 (1981).

C. D. Tesche, Bull. Am. Phys. Soc. 27, 266 (1982).

R. F. Voss, J. Low Temp. Phys. 42, 151 (1981).

R. F. Voss, R. B. Laibowitz, A. N. Broers, S. I. Raider, C. N. Knoedler, and J. M. Viggiano, IEEE. Trans. Magnetics MAG-17, 395 (1981).

R. F. Voss and R. A. Webb, Phys. Rev. Lett. 47, 265 (1981).

A. N. Vystavkin, V. N. Gubankov, L. S. Kuzmin, K. K. Likharev, V. V. Migulin, and V. K. Semenov, Phys. Rev. Appl. 9, 79 (1974).

This report was done with support from the Department of Energy. Any conclusions or opinions expressed in this report represent solely those of the author(s) and not necessarily those of The Regents of the University of California, the Lawrence Berkeley Laboratory or the Department of Energy.

Reference to a company or product name does not imply approval or recommendation of the product by the University of California or the U.S. Department of Energy to the exclusion of others that may be suitable.

TECHNICAL INFORMATION DEPARTMENT
LAWRENCE BERKELEY LABORATORY
UNIVERSITY OF CALIFORNIA
BERKELEY, CALIFORNIA 94720